Transportation Research Part C 169 (2024) 104876

Contents lists available at ScienceDirect

Transportation Research Part C

journal homepage: www.elsevier.com/locate/trc

Towards dynamic flight separation in final approach: A hybrid attention-based deep learning framework for long-term spatiotemporal wake vortex prediction

Nana Chu [a], Kam K.H. Ng [a,*], Xinting Zhu [b], Ye Liu [a], Lishuai Li [c], Kai Kwong Hon [d]

[a] *Department of Aeronautical and Aviation Engineering, The Hong Kong Polytechnic University, Hung Hom, Hong Kong Special Administrative Region, China*
[b] *School of Data Science and Hong Kong Institute for Data Science, City University of Hong Kong, Kowloon, Hong Kong Special Administrative Region, China*
[c] *School of Data Science, Department of Mechanical Engineering, City University of Hong Kong, Kowloon, Hong Kong Special Administrative Region, China*
[d] *Hong Kong Observatory, Hong Kong Special Administrative Region, China*

ARTICLE INFO

Keywords:
Flight separation
Aircraft wake turbulence
Recurrent neural network
Attention mechanism
LiDAR

ABSTRACT

The conservative and distance-based static wake vortex-related separation may restrict runway operational efficiency. Recent studies have demonstrated the potential of wake separation reduction under the Re-categorisation scheme of Aircraft Weight (RECAT). Furthermore, dynamic time-based flight separation considering vortex evolution with respect to aircraft pairs and meteorological conditions will be the ultimate objective for improving runway operational capacity without compromising safety. This paper presents a hybrid deep learning framework for aircraft wake vortex recognition, evolution prediction, and preliminary dynamic separation assessment in the final approach. Two-stage Deep Convolutional Neural Networks (DCNNs) are utilised to identify vortex locations and strength from wake images. Subsequently, we propose the Attention-based Temporal Convolutional Networks (ATCNs) for future long-term vortex decay and transport forecasts based on initial vortex information from DCNNs. 17,254 wake sequences generated by arrival flights at Hong Kong International Airport (HKIA) are used in this study. The proposed ATCN models outperform the specific benchmarks. Furthermore, the hybrid DCNN-ATCN model shows great benefits in mining both spatial vortex characteristics and temporal dependencies in vortex evolution, and achieves a computational speed of approximately 7 s per sequence. The final vortex duration assessment demonstrates a significant potential for separation reduction in the final approach when the crosswind speed exceeds 3 m/s. This study provides important implications for online and fast-time wake behaviour monitoring and state estimation. The results of vortex duration analysis conform to the RECAT-EU standards and present an efficient strategy for developing dynamic flight separation systems.

* Corresponding author.
E-mail addresses: na-na.chu@connect.polyu.hk (N. Chu), kam.kh.ng@polyu.edu.hk (K.K.H. Ng), xt.zhu@cityu.edu.hk (X. Zhu), ye.liu@connect.polyu.hk (Y. Liu), Lishuai.li@cityu.edu.hk (L. Li), kkhon@hko.gov.hk (K.K. Hon).

https://doi.org/10.1016/j.trc.2024.104876
Received 23 September 2023; Received in revised form 3 April 2024; Accepted 1 October 2024
Available online 10 October 2024

1. Introduction

With the increase in air traffic demand after the COVID-19 pandemic (IATA, 2022), "Improving runway capacity and operational efficiency" has become an urgent issue in air traffic management. Currently, the wake-vortex-related flight separation for ensuring flight safety is proven to be conservative and static in distance, which severely restricts runway efficiency. Wake turbulence is generated behind aircraft as the by-product of flight lift and is a pair of counter-rotating trailing vortices in the far-wake (Breitsamter, 2011; Hallock and Holzäpfel, 2018). When the rear aircraft encounters wake turbulence generated by the preceding aircraft, a variety of hazards may arise, such as uncontrollable pitch or roll movement, and aircraft structural damage.

As the circulation intensity of wake turbulence is highly relevant to aircraft weight, the initial vortex separation is defined on four aircraft weight categories, as suggested by the International Civil Aviation Organisation (ICAO). Additionally, the European Organisation for the Safety of Air Navigation (EUROCONTROL) and Single European Sky ATM Research (SESAR) have worked on Time-based Separation (TBS), in which aircraft are separated based on time rather than distance to reduce separation in favourable wind conditions (SESAR, 2015). Recently, the aircraft weight re-categorisation scheme (RECAT) has also been proposed by collaborative research between organisations such as the Federal Aviation Administration (FAA), ICAO, the European Union Aviation Safety Agency (EASA) and industries. This enhanced time-based separation has been implemented as the RECAT-ICAO (ICAO, 2023), RECAT-EU that is endorsed by EASA (EUROCONTROL, 2018), RECAT-EU-PWS safety case that are proposed by EUROCONTROL (EUROCONTROL, 2023) based on RECAT-EU, and three-phased RECAT by FAA (FAA, 2016). This RECAT scheme has been implemented in several national airports, such as the Paris Charles de Gaulle Airport and Le Bourget airports (DSAN, 2018). An increase of 3-5 flights per hour in arrivals at London Heathrow Airport has been observed during period of intense headwind (NATS, 2018).

Nonetheless, this enhanced separation standard remains conservative, static, and weather-independent. As meteorological conditions, particularly winds, play a leading role in the presence and movement of wake vortices in the background atmosphere (Holzäpfel et al., 2021), the study of dynamic flight separation with respect to vortex transport in certain weather situations is warranted, which is also the final goal of the FAA Next Generation Air Transportation System (NextGen) until 2030 (FAA, 2020). From the runway operational perspective, static flight separation is mainly considered as hard constraints for typical Aircraft Sequencing and Scheduling Problems (ASSP) (Barea et al., 2024; Pang et al., 2024; Prakash et al., 2018), such as the most classical Constrained Position Shifting (CPS) substitution algorithm (Balakrishnan and Chandran, 2010), the alternative graph method (Samà et al., 2017), and the robust optimisation approaches (Ng et al., 2020) under the ICAO wake separation standard. With the reduction of flight separation minima, the RECAT-EU can deliver a 5 % to 8 % capacity gain for European airports with heavy traffic (EUROCONTROL, 2018). Predictably, the dynamic flight separation related to aircraft wake assessment can lead to more significant enhancements in throughput and efficiency (Diana, 2015).

Prior research on aircraft wake turbulence fell into two methodological categories: numerical simulation (Visscher et al., 2013) and physical modelling (Holzäpfel, 2006). Nonetheless, these physical model-driven methods are either extremely time-consuming or subject to specific parametrical consumptions. With the massive amount of wake data collected during actual flight by the Light Detection and Ranging instruments (LiDAR) (Köpp et al., 2005), data-driven deep learning has demonstrated advantages in aircraft wake vortex recognition (Holzäpfel et al., 2021; Shen et al., 2023), A two-stage deep learning framework was also proposed for estimating the location and strength of aircraft wake vortex with high performance in our previous study (Chu et al., 2024). However, these tentative explorations are limited to single-image recognition in the short time horizon. The long-term forecast of the whole vortex evolution process matters more for supporting dynamic runway operations.

Consequently, this research endeavours to explore the long-term data-driven wake evolution prediction through algorithm enhancement and model fusion strategy. It is anticipated that the proposed methodology will facilitate the development of time-based separation indicators in the final approach, thereby increasing runway throughputs and further reducing the workload of air traffic controllers despite the increased number of landing flights that they must manage. Specifically, the contributions of this paper are threefold:

1. In terms of the overall methodology, we develop a hybrid deep learning framework to enable online spatiotemporal vortex feature recognition and future evolution projection. The hybrid deep learning framework includes two parts: a two-stage DCNN framework that is adept at capturing spatial features of vortex locations and strength; and attention-based TCN models that are ideal for forecasting the long-term temporal dependencies in vortex transport and decay.
2. For model performance validation, the efficiency of the proposed ATCN models and hybrid DCNN-ATCN strategy is assessed using real flight data and wake data at the Hong Kong International Airport, encompassing several scenarios of background turbulence. This model fusion reveals superior performance compared to benchmarking methods.
3. In vortex duration assessment, both aleatoric uncertainty and epistemic uncertainty of the proposed model for predicting vortex location are characterised by Gaussian distribution. The dynamic separation minima regarding crosswinds are determined by the presence of vortices in the approach profiles and verified from several aspects. Our preliminary results of dynamic separation minima show compliance with the current RECAT-EU standard, and also indicate the effect of strong crosswinds on separation reduction.

Subsequent to this, Section 2 reviews related studies. Section 3 briefly introduces the dynamics of wake turbulence and LiDAR implementation at HKIA. Section 4 presents the methodology of this research. The setting and result analysis of the numerical study are demonstrated in Section 5. Section 6 discusses the results, managerial implementations of this research and future work. Section 7 concludes this paper.

2. Related studies

2.1. Model-based aircraft wake vortex prediction

Computational Fluid Dynamics and LiDAR are two practices that enhance the knowledge of wake pairs. Computational Fluid Dynamics (CFD) has evolved into a sophisticated instrument that facilitates the ongoing examination of wake vortex dynamics in various environmental and turbulence conditions, including those in close proximity to the ground (Robins and Delisi, 1996; Visscher et al., 2013). However, due to the limitations of computational speed and data scale in simulations, it is impracticable to apply CFD directly for aircraft spacing in runway operations.

Several theoretical vortex models are therefore proposed to depict aircraft wake behaviours from the perspective of physical dynamics based on relevant internal and external parameters, such as the Aircraft Vortex Spacing System (AVOSS) (Proctor, 1998), Probabilistic Two-phase Wake Vortex Decay model (P2P) (Holzäpfel, 2003) and Deterministic Wake Vortex Model (DVM) (Visscher et al., 2010). The physical relationships between inputs such as flight speed, aircraft weight, etc., and wake movement state can be interpreted through the model. Nevertheless, these analytical models rely on specific meteorological assumptions and operational factors, which could lead to discrepancies between predicted and observed flight scenarios. Furthermore, the implementation of these systems in dynamic and large-scale flight separation management and runway operations might be constrained by the computational speed.

This research aims to investigate the potential of wake evolution forecast through a data-driven deep learning approach. The time dependencies between initial wake features and their future evolution will be learnt and explained by recurrent neural networks or other deep learning models capable of generating fast-time and time-series predictions over a massive data volume.

2.2. Wake encounter risk analysis

Hazard assessment under situations where the following aircraft encounters wake vortices generated by the leading aircraft, considering the status of the following aircraft (aircraft weight, flight speed, wingspan, etc.) and the level of vortex strength, is critical for determining the wake separation (De Visscher et al., 2016). The Rolling Moment Coefficient (RMC) metric (De Visscher et al., 2015) is primarily used in the RECAT-PWS-EU to quantitatively compare the wake encounter severity between follower aircraft in different MTOW types, particularly in terms of aircraft rolling motion. This evaluative metric is appropriate in scenarios involving the presence of a sustained wake vortex on the runway. Wake separation can also be determined by examining the positions of wake vortices in situations where favourable winds are present to clear the flight path (Holzäpfel et al., 2021). Therefore, this study also investigates the dynamic wake separation in relation to crosswinds in terms of wake presence.

2.3. LiDAR for wake vortex measuring

Consequently, LiDARs are implemented for wake data collection, validation, and vortex behaviour monitoring in actual flights at several airports (Smalikho and Banakh, 2015; Wu et al., 2019). The LiDAR instrument identifies spectra data (the Doppler frequencies) or the radial wind data in the scan plane. The rapid inversion methods are thus required to recognise vortex positions and strength from the background wind field (Yoshikawa and Matayoshi, 2017). The Velocity Envelope (VE) (Holzäpfel et al., 2003) based on spectra data and Radial Velocity (RV) method (Li et al., 2020; Smalikho et al., 2015) based on primarily radial wind data are two primary methodologies for processing scans and calculating vortex location from the Continuous Wave LiDAR (Köpp et al., 2005) and the pulsed Doppler LiDAR (Thobois et al., 2016; Yoshikawa and Matayoshi, 2017).

The theoretical models, such as the Bernham-Hallock (Burnham and Hallock, 1982) and the Lamb-Oseen models, are fitted to retrieve the vortex circulation based on velocities and vortex positions. Other innovative methods are also proposed to solve the circulation, including the path integration method by integrating Doppler velocity distribution and the LOS (line-of-sight) (Li et al., 2020), and the algorithm that takes ground effect into account (Smalikho, 2019).

To the best of our knowledge, these processing algorithms are of a generic nature and are susceptible to noise introduced by background wind turbulence, resulting in inaccurate locating and intensity estimation. The stochastic nature of wake turbulence necessitates techniques applicable to a variety of meteorological conditions during actual operations. Most importantly, these methods may not be suitable for a large-scale operation that requires automatic, quick, and reliable vortex decoding in near- real time.

2.4. Deep learning-based wake vortex prediction

One prosperous solution is the emerging novel data-driven machine learning models. Deep learning networks, such as convolutional neural networks, are adept at feature mining of wake images. Support Vector Machine (Pan et al., 2020) and object detection algorithms (Shen et al., 2023) were employed for wake vortex existence identification. However, these researches deal with the qualitative aspect of vortex processing tasks. The convolutional neural networks with regression were employed for quantitative vortex recognition. These networks were used to capture the locations and strength of vortices, either independently (Wartha et al., 2022) or in an integrated manner (Chu et al., 2024).

In another aspect, there are few studies about the spatiotemporal vortex feature prediction in the data-driven model category. Recurrent Neural Network (RNN) is a typical model that introduces feedback loops for capturing temporal dependencies in vortex time series. To avoid gradient vanishing problems and capture long-term temporal dependencies, Long-short Term Memory (LSTM)

(Hochreiter and Schmidhuber, 1997) and Gated Recurrent Unit (GRU) (Chung et al., 2014) networks are proposed. There are several practices of LSTM (Shi et al., 2021) or hybrid recurrent networks (Pang et al., 2021; Shafienya and Regan, 2022) for flight trajectory projection.

Nevertheless, these recurrent networks exhibit several limitations, such as restricted parallelisation ability, limited short-term memory, absence of global context, and issues related to sequential computing overhead. The aforementioned concerns may be alleviated by the emergent self-attention mechanism and temporal convolution with dilation operation but without recurrent connections (Lea et al., 2016). Hence, this study aims to explore the algorithmic improvements for predicting the evolution of wake vortices in a data-driven manner.

3. Backgrounds

3.1. Characteristics of aircraft wake turbulence

Aircraft wake turbulence is a complex turbulent motion that relates primarily to the generating aircraft, meteorology and ground effect (Breitsamter, 2011). The initial vortex location and strength are determined by the flight status and configuration parameters, such as the aircraft weight, wingspan, lift distribution, and flight speed (Hallock and Holzäpfel, 2018). The decay and evolution process of wake vortices depends heavily on the meteorological conditions, including wind direction and speed, wind shear, turbulence, etc. A two-phase model was proposed to describe aircraft wake vortex decay in moderate turbulence (Holzäpfel, 2006). In the initial stage, wake vortices diffuse at a low speed, and the vortex strength controlled by the leading aircraft can be represented as:

$$\Gamma_0 = \frac{M_A g}{\rho b_0 V_A},\ \mathrm{b}_0 = sB \tag{1}$$

where M_A is the aircraft mass, ρ represents the air density, V_A is the airspeed of the aircraft, s is the load factor of the aircraft wingspan, and B is the wingspan.

The second phase is characterised by a rapid decline in vortex strength and height. Furthermore, the ground effect may manifest when the turbulence is in close proximity to the ground, resulting in a secondary wake vortex pair forming below and outside the initial vortices, which would lead the former to rebound (Holzäpfel and Steen, 2007; Wu et al., 2019).

The meteorological conditions, such as crosswind and the background wind turbulence, play a crucial role in specifying how long a vortex remains potentially hazardous and indicating the transport of the wake vortices, as depicted in Fig. 1. Specifically, when the crosswind is roughly equivalent to the initial descent speed, the upwind vortex is likely to halt over the runway, and the decay of the wake pair will be unequal (Lin et al., 2017; Xu et al., 2023). While in a strong crosswind without the adverse headwind, and the prevailing headwind over approximately 5 m/s, the wake vortex will quickly leave the approach path (Holzäpfel et al., 2021). Furthermore, the large-scale and heavy atmospheric turbulence extracts energy from wake vortices while simultaneously diminishing their strengths, thereby accelerating their decay.

3.2. LiDAR implementation at HKIA

The LiDAR instrument at HKIA is capable of tracking vortices below 500 m in altitude and over extensive horizontal distances. Four Leosphere Windcube200S LiDARs were deployed at the ends of the runways at HKIA to monitor wake turbulence during the final approach and initial departure, as shown in Fig. 2(a). Furthermore, the configurations and parameters of these LiDARs were refined to

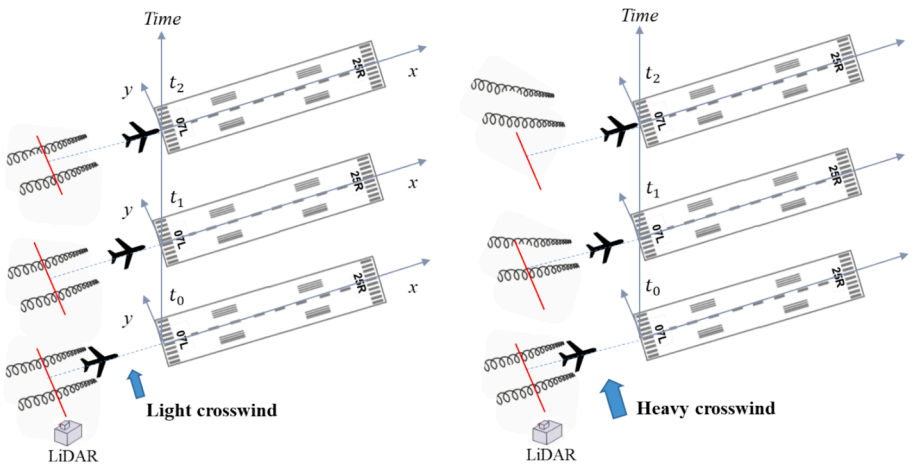

Fig. 1. The movement of wake vortices under crosswinds. (Left: vortex sink under light crosswinds. Right: significant lateral transport of vortices with sink under strong crosswinds).

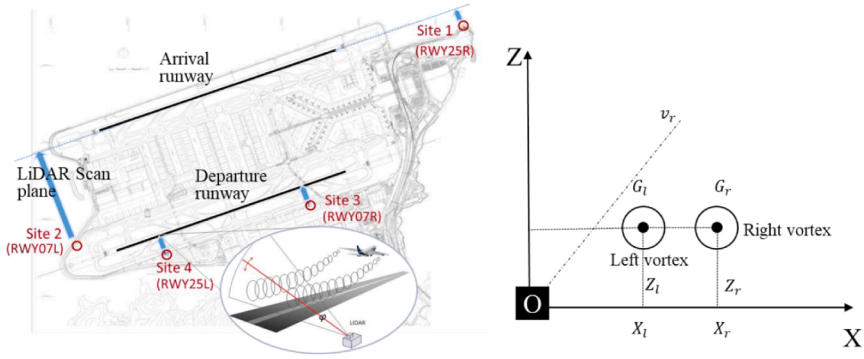

(a) Locations and scanning mode (b) Coordinate definition of wake positions

Fig. 2. LiDARs for aircraft wake vortex monitoring at HKIA.

accurately depict the entire path of wake vortices and their state of decay at HKIA. Each LiDAR scans in the mode of range height indicator from the top 35 ° to the bottom approximately every ten seconds and at the scan rate of 5 ° / s. The positions of the left and right vortices are defined using the Cartesian coordinate system, as shown in Fig. 2(b). More detailed information regarding wake LiDAR settings for the HKIA can be referred to in (Hon et al., 2021).

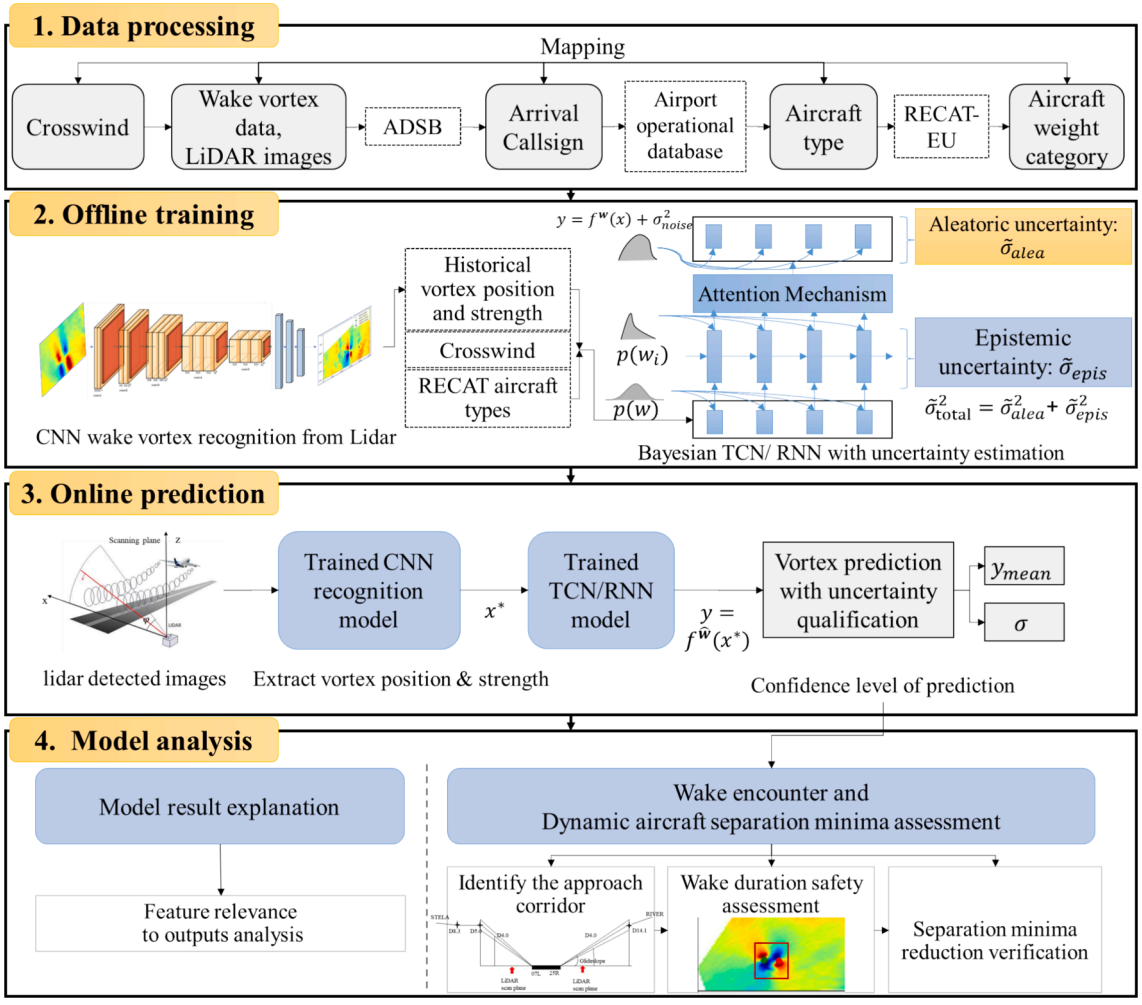

Fig. 3. Flowchart of the methodology for dynamic aircraft wake vortex recognition and evolution prediction.

3.3. LiDAR processing algorithm

The processing algorithm for Windcube200S is designed by LEOSPHERE to capture vortex locations and, consequently, retrieve vortex strength. Initially, the algorithm verifies the status of vortex presence based on radial wind speeds calculated from the RHI scans. Next, the locations of vortex cores are roughly estimated using an image processing technique and are finely optimised. Vortex strength is further retrieved by fitting the Hallock-Burnham model (Burnham and Hallock, 1982; Smalikho et al., 2015) on the Doppler spectra window that covers wake vortices. In addition to the generic parametric components of the Windcube200S processing algorithm (Smalikho et al., 2015; Thobois et al., 2016), the positions and specific parameters of these LiDARs at HKIA are fine-tuned and calibrated specifically to reduce estimation error and assure data quality in all weather conditions and for as many aircraft types as possible. Furthermore, it has demonstrated the aircraft hit rate of 89 %, overall mean error of 6 % and 9.9 % in wake span and initial wake strength measurement for two weeks (Hon et al., 2021).

4. Proposed method

4.1. Methodological framework

This research aims to develop an integrated deep-learning strategy that can be used to recognise wake vortices in real-time, anticipate vortex decay and estimate separation minima. This will be achieved by utilising historical wake vortex data derived from the LiDAR technique at the HKIA. The wake vortex recognition process involves quantifying vortex position and determining vortex strength based on LiDAR vortex images. The prediction of wake vortex evolution and decay provides insights into the future position and strength of vortices by utilising initial vortex data.

Fig. 3 depicts the methodological flowchart of this study with four primary stages. Firstly, the wake sequences are segmented with relevant flight information (flight speed, heading, aircraft type) from Automatic Dependent Surveillance-Broadcast (ADS-B) mapped and the ambient wind conditions considered. In the offline model training phase, the DCNN model for vortex recognition from LiDAR scans and Bayesian models (attention-based TCNs and RNNs) for predicting vortex evolution are built and trained. Subsequently, the trained DCNN and ATCN models are integrated and applied in real-time scenarios, in which the recognised vortex positions and strength in the initial three timesteps from DCNN are fed into the Bayesian attention-based TCN and RNN models for predicting vortex decay. The ultimate phase evaluates the dynamic minimum in aircraft separation concerning wind conditions in the final approach based on vortex duration analysis. In addition, feature importance analysis is employed to elucidate the model decision process, thereby bolstering the credibility of the deep learning model. The subsequent subsections will explain the model architectures and strategies pertaining to each component.

4.2. LiDAR data processing

The data derived from LiDAR for each scan contains two parts: the radial wind velocities, and values derived from the LiDAR processing algorithm (two-dimensional vortex locations relative to runway centrelines and height of LiDAR, and vortex intensity). The radial wind data are converted into heatmaps to visualise the whole vortex scope, where warm and cold colours indicate the positive and negative velocities relative to LiDAR, respectively. The relative positional deviations were converted into absolute values that are relative to LiDARs. Furthermore, the sequential vortex data with discontinuous scanning in time series and null values in each time step were removed, and these successive vortex scan data were segmented according to the characteristics of the initial and final wake vortices. In a stable ambient atmosphere, the wake vortices generated by heavy aircraft can persist for a dozen lidar scans, lasting for several minutes. In the wake vortex series with more than 12 timesteps, a significant proportion is attributed to the superposition of

Table 1
Inputs and outputs of the DCNN model for vortex recognition and TCN models for vortex sequential prediction.

Model	Input/output	Feature variables	Description	Unit
CNN model	Inputs	Wake images	Images of LiDAR scans in the first three timesteps	–
	Outputs	$\widehat{X}_l^{(t_0-t_2)}, \widehat{X}_r^{(t_0-t_2)}$	Predicted lateral positions of vortex cores in the first three timesteps	m
		$\widehat{Z}_l^{(t_0-t_2)}, \widehat{Z}_r^{(t_0-t_2)}$	Predicted vertical positions of vortex cores in the first three timesteps	m
		$\widehat{G}_l^{(t_0-t_2)}, \widehat{G}_r^{(t_0-t_2)}$	Predicted strength in the first three timesteps	m^2/s
TCN models	Inputs	$X_l^{(t_0-t_2)}, X_r^{(t_0-t_2)}$	Reference lateral positions in the first three timesteps	m
		$Z_l^{(t_0-t_2)}, Z_r^{(t_0-t_2)}$	Reference vertical positions in the first three timesteps	m
		$G_l^{(t_0-t_2)}, G_r^{(t_0-t_2)}$	Reference strength in the first three timesteps	m^2/s
		$v_{lat}^{(t_0-t_2)}$	Average crosswind in the first three timesteps	m/s
		RECAT	The recategorised aircraft weight category in consistent with RECAT-EU	–
	Outputs	$\widehat{X}_l^{(t_3-)}, \widehat{X}_r^{(t_3-)}$	Predicted lateral positions in future timesteps	m
		$\widehat{Z}_l^{(t_3-)}, \widehat{Z}_r^{(t_3-)}$	Predicted vertical positions in future timesteps	m
		$\widehat{G}_l^{(t_3-)}, \widehat{G}_r^{(t_3-)}$	Predicted strength in future timesteps	m^2/s

two wake vortices resulting from errors in the automatic segmentation process of these vortices. Therefore, to ensure the accuracy of wake vortex forecasting, vortex sequences with a duration time of less than 4 timesteps and over 12 timesteps were removed.

In addition to the wake vortex data, crosswind speed from the background turbulence is also considered as the main ambient feature. The average crosswind on each LiDAR scan is computed by the Leosphere data processing algorithm, with the same time interval as the LiDAR scan. Furthermore, the flight information (approaching speed and aircraft type) of the final approach from the ADS-B was also cleaned and mapped with each wake sector according to timestamps and three-dimensional positions when the flight approaches the LiDAR scan plane. To coordinate with the latest aircraft weight classification standard, the aircraft types extracted for each wake sequence were mapped to the weight categories in RECAT-EU.

To summarise, for the historical vortex data of a flight denoted as $X = \{x_1, x_2, \cdots, x_n\}$, x_i represents features in timestep i, the input features for training the DCNN model and the time-series prediction model, as well as their respective outputs, are listed in Table 1. To improve prediction accuracy and utility, the length of the historical feature window is defined as three timesteps ($t_0 - t_2$) for predicting targets in future timesteps. For LiDARs in Site 1 and Site 2, the time intervals in each timestep are approximately 12 s and 9 s, respectively.

4.3. Proposed models

4.3.1. Deep convolutional neural networks

For aircraft wake vortex recognition, deep convolutional neural networks employing multiple convolutional modules and heatmaps from LiDAR scans are utilised to extract the location of vortex cores and the strength of vortex pairs. The two-stage DCNN models proposed in our previous work (Chu et al., 2024) are used in this paper to process the initial wake information required for vortex decay prediction in real flight scenarios. The initial phase of this framework focused on the estimation of two-dimensional vortex location from the raw entire wake vortex images. Further, the crucial image areas that are primarily associated with vortex circulation were cropped according to the projected locations of vortex cores, which were then used for vortex strength estimation in another DCNN model.

4.3.2. Attention-based TCN models

After the relevant aircraft wake vortex features and atmosphere features are derived, we proposed the novel one-dimensional dilated convolutional operations with an attention mechanism for efficient and high-performance sequential vortex feature prediction. The overall methodological framework of the proposed models is illustrated in Fig. 4. Remarkably, two remarkable attention-based TCN models are proposed, which consist of three main modules: dilated convolutional residual block and multi-head attention module or Convolutional Block Attention Module (CBAM). To distinguish between the simple TCN model and the attention-based

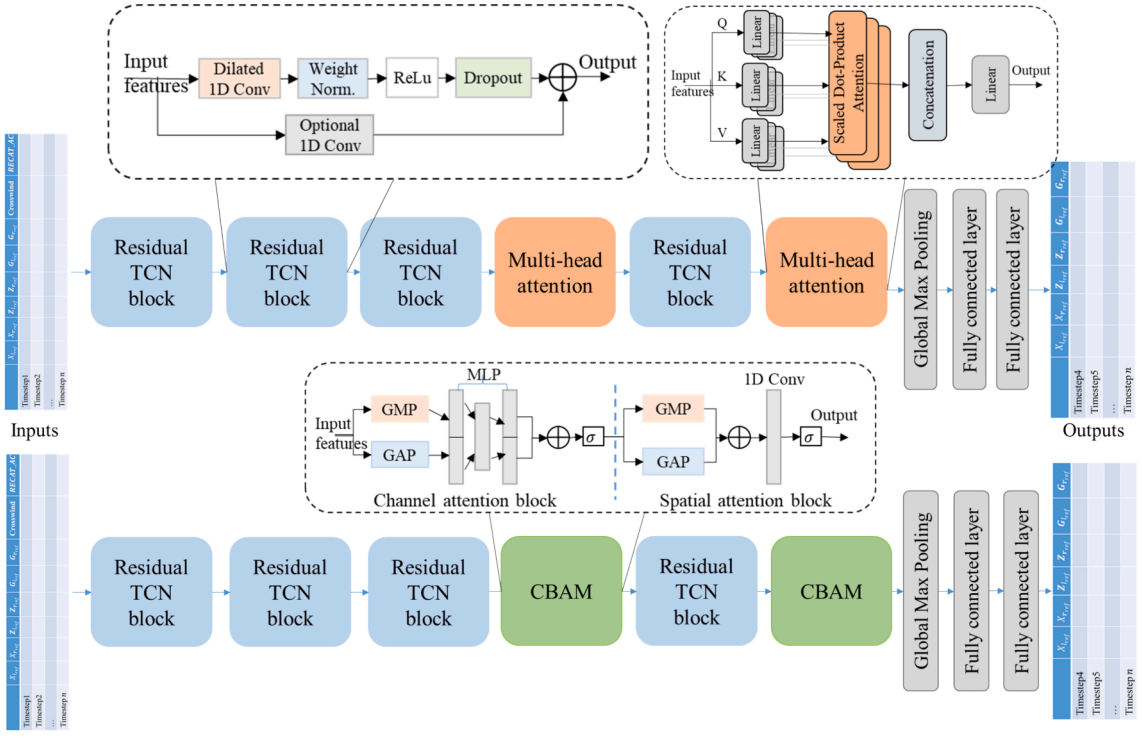

Fig. 4. Overall methodological framework of proposed attention-based TCN models for vortex decay projection.

TCN models, the TCN model with multi-head attention mechanism is named multi-head attention-TCN (ATCN in following experiments), and the model with CBAM module is called the CBAM-TCN.

(1) **Residual temporal convolutional module**.

In the above hybrid model, one essential component is the temporal convolutional module, where the parallelism dilated convolutions achieve great computational efficiency compared to traditional recurrent neural networks. Notably, the dilated convolutions enable the receptive field of the network to grow exponentially with the number of layers and manipulate how many positions the convolutional kernel skips. Specifically, for the above two-dimensional sequential vortex data X with a timespan of l, $X = \{x_1, x_1 \cdots, x_t, \cdots, x_l\}, x_i \in R^n$ and filters $f : \{0, \cdots, k-1\}, k \in R$, the dilated convolution F on sequence element x_t can be denoted as:

$$F(x_t) = (X *_d f)(t) = \sum_{i=0}^{k-1} f(i) \bullet X_{t-d \bullet i} \tag{2}$$

Where d denotes the dilation factor, k represents the kernel size, and $s - d \bullet i$ is the direction of the past. Consequently, the output of dilated convolution will be: $\widetilde{X} = (F(x_1), F(x_2), \cdots, F(x_l))$.

After the dilated convolution, the weighted normalisation and dropout will be applied to the extracted features $\widetilde{X}$, with the output denoted as $H\left(\widetilde{X}\right)$. Finally, the summation of operated outputs and the initial input, denoted as $G(x)$, can be formulated as $H\left(\widetilde{X}\right) + X$, and will be taken as input for the subsequent residual module or attention module.

(2) **Multi-head self-attention mechanism**.

To further improve the ability of long-term temporal dependencies, the multi-head self-attention mechanism is added after the final two residual convolutional blocks for capturing the most critical information and relationship of the elements in the feature space, thus further enhancing model performance and general ability. Specifically, for the sequence of embeddings ($G(x)$), three linear projections will be operated to obtain the query (Q), key (K) and value (V) vectors for each token in the sequence. Then, for each position in the input sequence, the attention is denoted as

$$Attention(Q, K, V) = softmax\left(\frac{QK^T}{\sqrt{d_k}}\right)V \tag{3}$$

Furthermore, in multi-head attention, the above attention layers, or heads, will be performed in parallel for k times, concatenated and then projected to get the final output.

$$head_i = Attention(Q_i, K_i, V_i) i = 1, 2, \cdots .k \tag{4}$$

$$MultiHead_{output} = Concat(head_1, head_2, \cdots head_k) W_o \tag{5}$$

Where W_o is the learned matrix of the model parameter.

(3) **Convolutional block attention module**.

Another solution for attention is the convolutional block attention module, which is an innovative architecture component designed to enhance the capabilities of convolutional networks. It sequentially combines both channel and spatial attention mechanisms to enrich the feature representations, allowing the network to focus on the most relevant regions (Woo et al., 2018). Specifically, to capture the channel-wise attention after one-dimensional convolutions in our model, the average pooling and max pooling are employed in parallel to learn the distinctive object features, F^c_{avg} and $F^c{}_{max}$ respectively. Next, each descriptor is forwarded to a shared multi-layer perceptron (MLP), and then their results are merged using element-wise summation and operated with sigmoid function to get the one-dimensional channel-wise attention map $M_C(F)$.

$$M_C(F) = \sigma\left(W_1\left(W_0\left(F^C_{avg}\right)\right) + W_1\left(W_0\left(F^C_{max}\right)\right)\right) \tag{6}$$

Where W_0, W_1 denotes the weights of MLP layers, and σ is the sigmoid function.

In addition, to identify where the two-dimensional feature map matters, the one-dimensional spatial attention map in this study ($M_s(F)$) is generated across the channel, by one convolutional layer over the concatenated average-pooled and max-pooled features.

$$M_s(F) = \sigma\left(f^2\left(\left[F^C_{avg}, F^C_{avg}\right]\right)\right) \tag{7}$$

Where f^2 represents the one-dimensional filter with a size of 2, and σ denotes the sigmoid function.

4.3.3. Uncertainty estimation with Bayesian neural network

Compared to the single-point output prediction, the probabilistic vortex location and strength estimation with a high confidence level is anticipated to be implemented in safety–critical aircraft traffic operations. Therefore, this study also considers both aleatoric uncertainty that comes from the inherent noise or randomness in the data, and the epistemic uncertainty resulting from limited training data and model architecture in our tasks. These two kinds of uncertainty can be learnt from the Bayesian inference perspective.

The total predictive uncertainty $V(y|x)$ can be computed by integrating these two kinds of uncertainties:

$$V(y|x) = V(E(f(x,\Theta))) + E[V(y|x,\Theta)] \tag{8}$$

where the first term is the variance of the predicted means of the Bayesian model and represents the epistemic uncertainty, and the second term is the average of the model's predicted variance, which indicates the aleatoric uncertainty. Detailed information about uncertainty modelling can be referred to Appendix A.

To distinguish between the model with a single-point forecast and the model that considers uncertainty estimation, the model without uncertainty simulation is defined as the deterministic DCNN model or ATCN model; otherwise, it is called the probabilistic model.

4.3.4. Model fusion strategy

The aforementioned DCNN models are adept at data mining from wake vortex images, indicating their suitability for vortex monitoring in near real-time. However, to support advanced runway operations, it is anticipated that the future duration of vortices can be estimated when only the initial vortex images are captured by LiDAR. Therefore, the fusion of DCNN and ATCN is proposed to integrate the advantages of these two models in both capturing spatial features and identifying temporal dependencies, thereby achieving both superior performance and long-term prediction capability in vortex recognition and evolution prediction.

4.4. Exploratory evaluation of wake presence in the final approach path towards dynamic wake separation

As wind conditions play a leading role in the descent and transport of wake vortices, strong winds and unstable atmospheric turbulence may expedite the decay, blowing vortices away from runway centrelines to the left or right side. If so, the wake separation may be reduced in these instances. Therefore, based on the above probabilistic and reliable vortex evolution prediction under the developed models, the potential of aircraft separation minima reduction can be verified through duration assessment of vortex presence.

The duration of vortex presence in the above circumstances is evaluated upon the determination of standard approach profiles in LiDAR scan planes. In addition to the allowable approach paths calculated for instrument landing rules in (Chu et al., 2024), the lateral and vertical boundaries of the approach profiles were loosened to achieve an initial vortex coverage of more than 80 %, as shown in Table 2.

Notably, the above approach profiles are defined for flights at low altitudes and under steady wind conditions. In the presence of wake vortices in the approach corridor at all times (typically in a stable atmosphere or with weak crosswinds), further separation reduction must be evaluated in light of the wake encounter risk, which requires consideration of vortex intensity and following aircraft (De Visscher et al., 2016). As the performance of vortex strength estimation is quite worse than vortex location prediction, the separation reduction is illustrated only in terms of the cleanliness of the approach profiles, encompassing the following two aspects:

(1) Get the positional boundaries of the two-dimensional vortex cores with a 95 % confidence level through the probabilistic TCN model with the best performance.
(2) Determine the last timestep that the entire wake pair is outside of the approach profiles, either laterally or vertically, considering also the regions of wake turbulence and a safety margin. Therefore, separation reduction evaluated in this study occurs exclusively when the anticipated wake duration is shorter than the lifecycle of the wake as detected by the LiDAR.

5. Numerical study

This section presents the training configuration of the two-stage DCNN model and the attention-based TCN models, and illustrates the performance of proposed models in location and strength projection of aircraft wake vortices at the HKIA. Furthermore, we also verify the applicability of the developed model in exploring the dynamic flight separation minima under vortex duration analysis.

Table 2
The height and horizontal position range of aircraft at the LiDAR scanning plane.

Runway	LiDAR distance (m) to Runway (x profile)	LiDAR distance (m) to Runway (y profile)	Estimated allowable range of height (m) to ground	Estimated allowable range of height (m) in LiDAR plane	Estimated allowable range of horizontal position (m) in LiDAR plane	Coverage percentage of initial wake vortices
07L	1400	1116.31	56.84—91.40	35—84.40	±120	96 %
25R	275	1511.99	72.72—116.93	50—109.93	±120	81.69 %

5.1. Model training and evaluation configuration

A total of 17,254 wake vortex sequences from arrival flights at the HKIA, consisting of 108,377 timesteps from June to October 2019, were captured by LiDARs Site 1 and Site 2, and then processed for this study. As the evolution of wake vortices is forecasted through time series analysis in this study, all processed historical wake sequences were split into training, validation and test datasets randomly by sequence flags in the proportion of 6:2:2. This guarantees the ability to acquire knowledge of wake vortices produced by various aircraft types and background atmospheres. The short-term prediction described in this paper represents a single-timestep forecast for roughly 10 s. The term "long-term prediction" refers to a series of forecasts in the next several steps that, dependent on the vortex lifespan detected by LiDAR, may last for one to two minutes.

All experiments in this paper were conducted on a Windows 10 desktop with an Intel Core i7-12700 K processor, NVIDIA GeForce RTX 3060Ti GPU (1.78 GHz), and DDR5 RAM with 32 GB. Before model training, input and output data were normalised using the MinMaxScaler. Grid search was performed to tune the hyperparameters and relevant parameters of these models, such as the batch size and model layers. The training process employs the Adam Optimiser and has a decayed learning rate of 0.95 in every 30 epochs. The DCNN models were trained for up to 500 epochs, and the attention-based TCN models were trained for up to 1000 epochs. The early stopping technique is applied to identify model parameters with the best performance.

Both the Mean Absolute Error (MAE) and Root Mean Square Error (RMSE) metrics are used for model performance evaluation, with their formulas as below:

$$MAE = \frac{1}{n}\sum_{i=1}^{n}|y_i - \hat{y}_i| \tag{9}$$

$$RMSE = \sqrt{\frac{1}{n}\sum_{i=1}^{n}(y_i - \hat{y}_i)^2} \tag{10}$$

where n is the number of data points in the dataset, y_i is the vector of true target values, and $\hat{y}_i$ is the vector of predicted values.

5.2. Model performance assessment

Under the same experimental conditions and test dataset, the performance of the proposed attention-based TCN models is compared to that of benchmarking models. This comparison encompasses the short-term prediction performance on a single test dataset and the average performance under 5-fold cross-validation, the performance of long-term prediction and the model hybrid.

Performance of ATCN models in short-term prediction horizon: Table 3 demonstrates the superior performance of the proposed two attention-based TCN models, especially the TCN model with a multi-head attention mechanism, compared to the pure TCN model and two typical recurrent neural networks. The dilation convolutions exhibit a broader range of temporal dependencies, with efficient utilisation of features in the time window. Moreover, the attention mechanism further improves the feature mining process. Specifically, the multi-head attention-based TCN model achieves nearly 68 % and 70 % MAE reduction in X_l and X_r prediction, compared to GRU and LSTM, respectively. To achieve a comprehensive assessment of model generalisation performance and avoid the variance associated with single-fold validation, we also applied the 5-fold cross-validation to evaluate the average performance of these models across five partitions in Table 4. It also indicates the best performance of the ATCN models in lateral position prediction despite a decline in performance gains. Nevertheless, the improvement in strength estimation performance in ATCN and CBAM-TCN models is less significant than that of location estimation, as identifying vortex circulation is more challenging, resulting in more significant errors in the initial measurement.

In essence, this improvement can be demonstrated through feature relevance visualisation with SHAP values (Lundberg and Lee, 2017) by providing insights into how different features impact the prediction outcomes. The positive SHAP values indicate that the corresponding feature has a positive impact on increasing the prediction value, while negative values indicate the opposite. In Fig. 5 and Fig. 6, for each location output, the left figure represents the influence of each feature on the output for a specific individual input sample. They provide detailed insight into how historical locations and other features in the input impact prediction for this sample. Nonetheless, the right figure, which is the summary plot, intuitively shows the importance ranking of all features in the overall test

Table 3
Test performance comparison of the proposed models for short-term vortex position and strength prediction (Best performance in bold).

Deterministic model	Vortex location estimation								Vortex strength estimation			
	MAE (m)				RMSE (m)				MAE (m^2/s)		RMSE (m^2/s)	
	XL	ZL	XR	ZR	XL	ZL	XR	ZR	GL	GR	GL	GR
ATCN	**8.32**	**4.48**	**8.72**	**4.47**	**11.68**	**6.53**	**12.36**	**6.59**	**48.86**	**49.06**	**66.74**	**65.03**
CBAM-TCN	**10.45**	**4.52**	**9.93**	**4.52**	**13.58**	**6.57**	**13.28**	**6.64**	49.07	**49.16**	67.08	65.66
TCN	11.37	4.58	11.12	4.64	15.35	6.58	15.01	6.57	**48.95**	49.17	**66.78**	**65.42**
GRU	27.75	9.61	27.19	9.82	36.24	13.12	35.50	13.64	50.11	50.38	67.48	66.12
LSTM	28.44	9.35	28.10	9.65	38.33	13.49	36.14	14.41	70.44	69.56	88.82	86.63

Table 4
5-fold cross-validation of the proposed models in wake vortex location estimation (Best performance in bold).

Deterministic model	Vortex location estimation							
	MAE (m)				RMSE (m)			
	XL	ZL	XR	ZR	XL	ZL	XR	ZR
ATCN	**11.724**	**4.54**	**11.406**	**4.584**	**15.226**	**6.642**	**14.98**	**6.61**
CBAM-TCN	**13.712**	5.476	**12.294**	**5.118**	**17.678**	8.602	**16.178**	7.508
TCN	20.752	**4.616**	23.956	4.64	26.342	**6.682**	29.932	**6.662**
GRU	31.716	9.506	30.948	9.88	39.876	12.826	40.512	13.4
LSTM	34.918	9.738	36.174	10	46.022	12.942	46.91	13.472

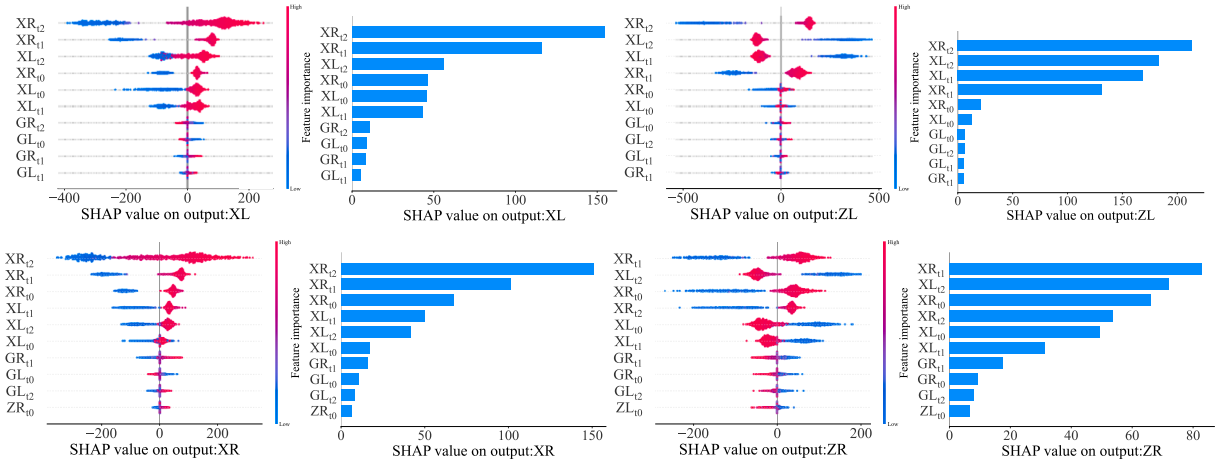

Fig. 5. Relevance of features to outputs of the multi-head attention-based TCN model based on the SHAP kernel explainer.

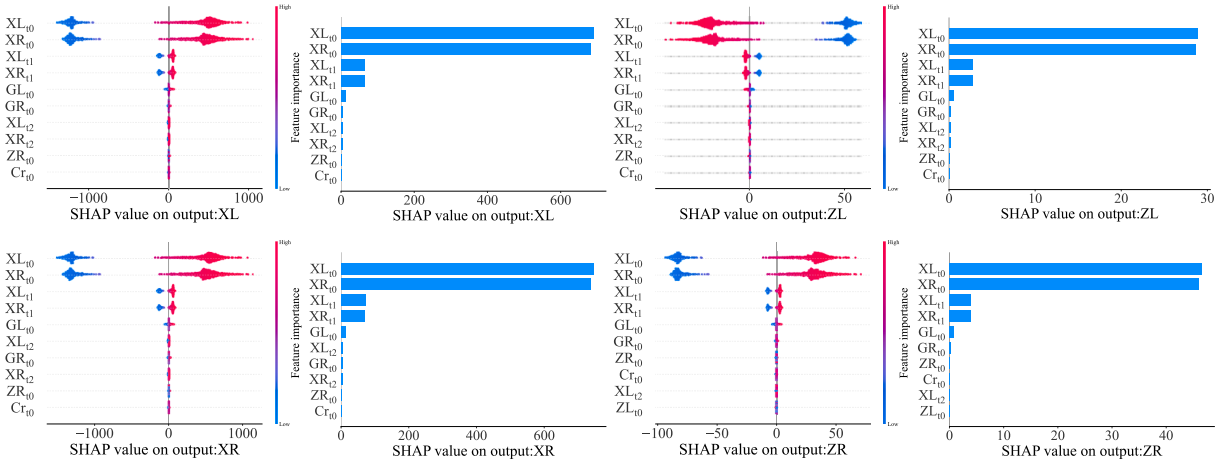

Fig. 6. Relevance of features to outputs of the LSTM model based on the SHAP kernel explainer.

dataset, as well as the impact of each feature on the prediction.

Fig. 5 demonstrates that the most relevant vortex features for future location prediction in the ATCN model span all timesteps in the input feature window (8×3 dimensions with 8 features in three timesteps), while the LSTM model depends primarily on input in the first timestep and achieves the worst prediction performance, as depicted in Fig. 6. More specifically, the features of lateral positions in the first three timesteps not only lead the forecast of their future values but also more intriguingly, play a leading role in future vortex height prediction. In addition, the decay of strength also correlates strongly with vortex height reduction, which reveals the coupling relationship between the horizontal and vertical positions of the vortex pair.

The above results can also be interpreted in relation to vortex physics despite the learning process being different from the mechanism of vortex physics. The dynamics of wake vortices involve not only instantaneous positions but also historical information

(the increment of lateral positions or lateral movement speed) for future vortex position prediction. Furthermore, changes in lateral positions can impact vortex height, indicating a coupling between horizontal and vertical positions in vortex evolution. The strong correlation between strength decay and vortex height reduction also aligns with known vortex physics principles. As a vortex weakens over time (due to diffusion or other factors), its height tends to decrease, reflecting the energy dissipation and spreading characteristics of wake vortices.

The performance of the ATCN model in long-term prediction horizon: Table 5 verifies the online and long-term prediction ability of the attention-based TCN models trained offline. As vortex location prediction is more accurate than intensity estimation, it is more reliable and usable for runway operations. Therefore, wake locations are the focus of research on long-term decay prediction and hybrid models for online prediction. The overall MAEs of the ATCN model in long-term lateral location projection are similar to those of the pure TCN model, and are reduced by around 40 % when compared to GRU and LSTM. Moreover, although Fig. 7 suggests that prediction errors may increase as the length of the vortex sequence increases, the ATCN model achieves considerable low-level MAE in the lateral position, specifically approximately 37 % and 45 % less than GRU and LSTM, respectively, for vortex sequences consisting of 9—12 timesteps. It is worth mentioning that the long-term prediction in this study is conducted on wake sequences with no more than 12 timesteps to guarantee the quality of wake segmentation. Additional detailed analyses can be performed to investigate vortex behaviour in the second stage with consideration of the ground effect when high-quality and long-lifetime wake sequences are available.

As model performance at high crosswinds is crucial for further separation assessment, we also analysed model performance under different levels of crosswind speeds. Wake sequences from January to April 2019 were incorporated into the above test dataset for evaluating crosswinds. Fig. 8 demonstrates model performance comparison under 800, 800, 800, and 569 wake sequences with absolute crosswinds of 0–2, 2–4, 4–6, and 6–8 m/s, respectively. These data are independent of the above training and validation datasets. The quantity of wake sequences under absolute crosswinds exceeding 8 m/s is small and is therefore disregarded. The results show an evident trend of MAE reduction with the increase of crosswind speeds for all models. Notably, the ATCN model exhibits a superior performance, leading credibility to its application in separation suggestion.

The performance of model fusion strategy for both vortex recognition and future prediction: Table 6 shows the results of model fusion for online wake vortex prediction with initial vortex data captured from DCNN models. With the highly accurate vortex locations and intensity estimated by DCNNs, the ATCN model and the TCN model obtain over 27 % and 11 % performance enhancement in the long-term X_l and X_r prediction, compared to the other benchmarks. Nonetheless, the CBAM-TCN model achieves a worse performance with more computational time. Notably, wake sequences with lengths of more than 9 timesteps have an approximately 15 % additional MAE reduction compared with the results from the shorter sequences in the CNN-TCN fusion strategy. One reason behind this is the superior recognition accuracy of the DCNN model on initial vortex images generated in a more stable atmosphere, which thus lasts for a long time. In addition, the computational speed of the long-lifetime vortex sequences gets to an average of 7.76 s per sequence, which provides strong preconditions for near real-time and online vortex monitoring and flight

Table 5
Long-term prediction performance of the proposed models under different vortex lengths.

Deterministic Model	Number of wake seq.	Seq. length (time steps)	MAE (m)				RMSE (m)			
			XL	ZL	XR	ZR	XL	ZL	XR	ZR
ATCN with roll prediction	1575	4—12	17.07	6.49	18.98	6.70	27.09	9.43	30.29	10.91
	567	4 – 6	**10.73**	6.10	**11.27**	**6.38**	**15.11**	8.67	**15.61**	**9.33**
	592	6—9	15.33	**6.01**	16.57	**6.22**	23.04	**8.30**	24.96	9.49
	416	9 – 12	19.75	6.97	21.79	6.93	30.37	10.16	34.00	9.84
TCN with roll prediction	1575	4—12	16.35	6.29	16.53	6.58	23.54	9.02	24.11	9.75
	567	4 – 6	**12.16**	5.99	**12.35**	6.45	**16.99**	8.65	16.97	**9.34**
	592	6—9	15.35	**5.96**	15.78	6.33	22.12	**8.29**	22.74	9.54
	416	9 – 12	18.32	6.63	18.30	6.81	26.08	9.65	26.72	10.02
CBAM-TCN with roll prediction	1575	4—12	24.92	6.62	21.98	6.97	35.6	9.57	31.84	10.48
	567	4 – 6	13.88	6.12	12.85	6.46	18.58	8.75	**16.90**	9.56
	592	6—9	20.03	6.12	19.57	6.41	27.40	8.47	26.96	9.63
	416	9 – 12	30.30	6.90	26.73	7.28	42.83	9.79	38.60	10.27
GRU with roll prediction	1575	4—12	29.02	9.50	29.54	9.70	38.56	13.01	40.29	13.51
	567	4 – 6	27.09	9.67	25.63	9.55	34.82	13.12	34.71	13.06
	592	6—9	30.29	11.33	25.37	11.62	36.91	15.15	31.66	16.17
	416	9 – 12	31.16	9.34	29.17	9.57	40.95	12.83	39.42	13.26
LSTM with roll prediction	1575	4—12	31.16	9.36	29.01	9.65	42.34	13.49	37.53	14.41
	567	4 – 6	24.55	11.99	27.31	11.07	30.20	16.20	33.09	16.53
	592	6—9	26.95	8.92	27.96	9.16	35.10	11.89	36.37	11.92
	416	9 – 12	37.04	8.95	30.50	9.66	50.76	13.96	39.80	15.74

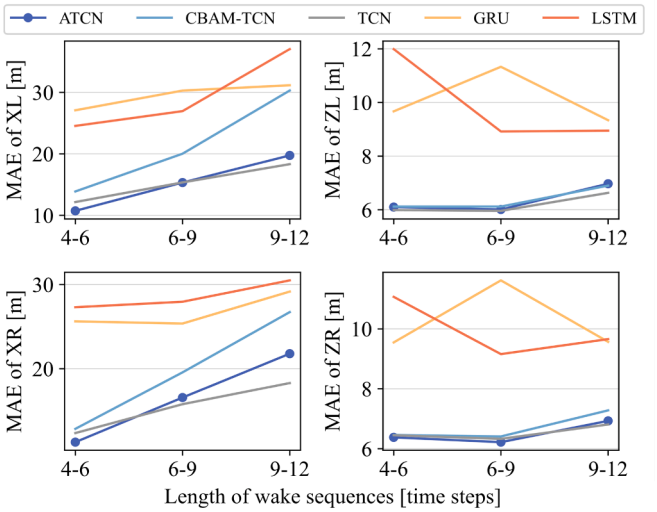

Fig. 7. Performance comparison of proposed models and benchmarking models based on the same test dataset with different wake sequence lengths.

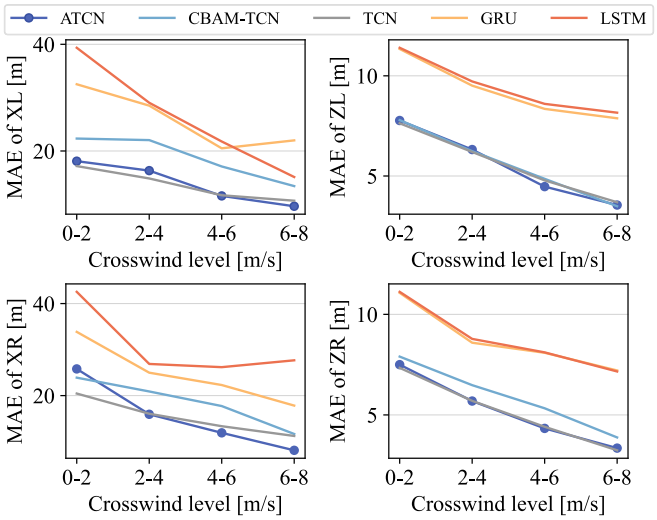

Fig. 8. Performance comparison of proposed models and benchmarking models based on the same test dataset under different levels of crosswinds.

Table 6
Performance of CNN-TCN/LSTM/GRU models in long-term prediction of vortex evolution based on wake recognition for real flight scenarios.

Deterministic Model	Number of wake seq.	Seq. length (time steps)	MAE (m)				RMSE (m)				Computation time (min)
			XL	ZL	XR	ZR	XL	ZL	XR	ZR	
CNN-TCN	100	4–12	**20.99**	**7.05**	**22.52**	**6.99**	**29.07**	**9.65**	**34.31**	**9.49**	21.14
	904	9–12	**17.73**	**8.18**	**17.10**	8.27	**26.54**	11.78	**25.65**	12.27	117.07
CNN-ATCN	100	4–12	22.70	7.45	24.76	**6.45**	36.50	10.05	41.04	**8.95**	22.53
CBAM-TCN	100	4–12	25.81	6.91	25.89	6.71	35.72	**9.52**	39.77	9.41	34.96
CNN-GRU	100	4–12	33.81	8.93	31.23	9.09	42.37	11.16	43.56	11.45	20.80
CNN-LSTM	100	4–12	31.28	10.64	29.10	10.50	40.18	17.93	37.72	16.17	21.14

separation suggestion, thereby supporting efficient runway operational decisions.

Following are three typical wake sequences lasting for 7, 9 and 12 timesteps in absolute crosswinds of 0.23, 2.08 and 5.9 m/s, respectively. The results of vortex recognition and evolution prediction from our proposed hybrid CNN-ATCN model are visualised accordingly. For wake vortices generated in a stable atmosphere and lasting for a long time, as depicted in Fig. 9 and Fig. 10, the rapid

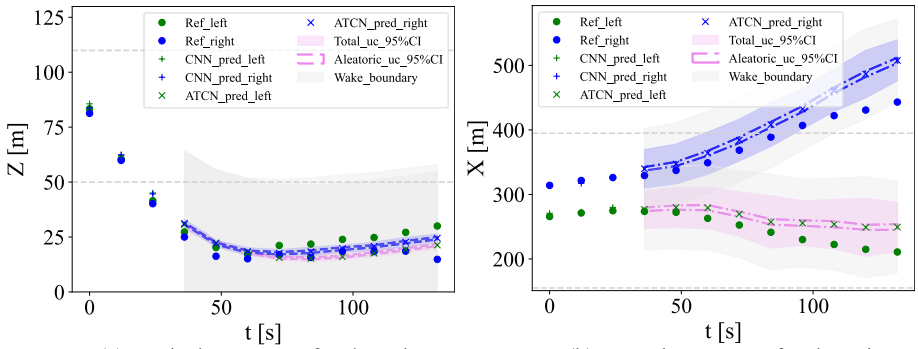

(a) Vertical transport of wake pair (b) Lateral transport of wake pair

Fig. 9. Visualisation of the long-term prediction results of the CNN-ATCN model for a vortex sequence generated by aircraft in the CAT-B category under mean crosswind of 0.23 m/s during 2019/08/16 17:34:04 – 17:36:18.

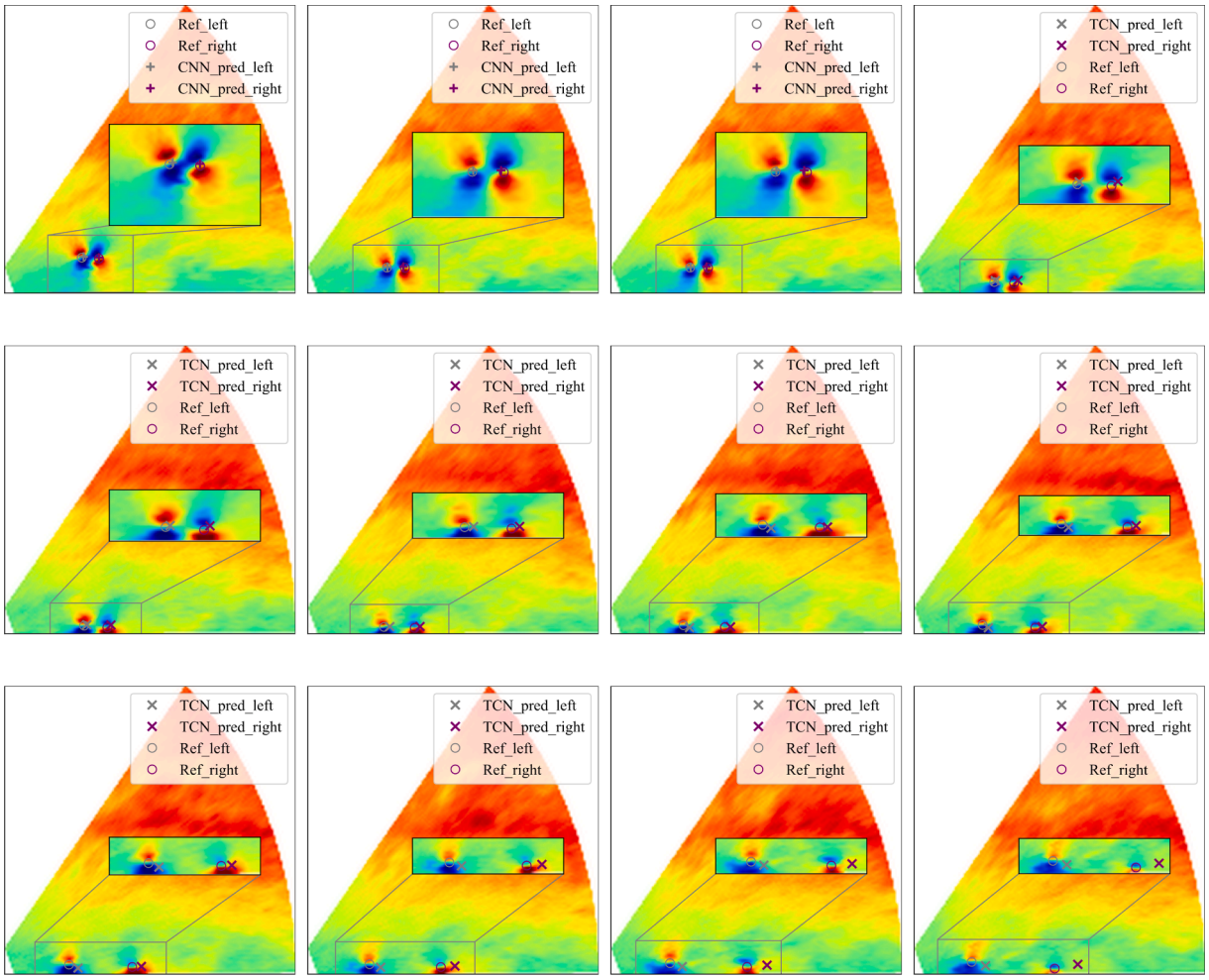

Fig. 10. Visualisation of the predicted results of Fig. 9 in LiDAR wake images.

vortex decay and sink in the first stage are evident with high prediction accuracy (timestep 4–8), while the second phase, starting from the 9th timestep, achieves increased errors, especially for the lateral position. The green and blue colours in the figure indicate the left and right vortex. The solid dot, "+" and "x" markers represent the ground truth of location, and the predicted results of CNN and ATCN models, respectively. Furthermore, both the aleatoric uncertainty and total uncertainty considering epistemic uncertainty in 95 % confidence interval are visualised in pink and blue colour with dot-dash lines. The grey area represents the region of wake vortices with

consideration of vortex radius that relates to aircraft wingspan. The dotted lines in Fig. 9 represent the allowable approach profiles. Given the perpetual presence of a wake vortex within this profile, separation reduction in this scenario is not feasible.

Fig. 11 and Fig. 13 indicate that even for wake pairs generated under unstable background turbulence (Fig. 12), the prediction of vortex transport and descent in the short term also achieves high accuracy. Although the long-term prediction of vortex cores is not so accurate, the consideration of positional uncertainty and a safety margin in the wake region improves reliability. Moreover, there is a remarkable and rapid lateral movement of the whole wake pair till they move outside of either the left or the right of the approach profile. The strong crosswind blows the wake pair laterally, as illustrated in Fig. 13(c), which results in a clean approach profile.

5.3. Exploratory evaluation of aircraft separation minima reduction in the final approach

The above probabilistic ATCN model with long-term prediction ability is expected to provide reliable vortex locations to further support dynamic flight separation. For the above three scenarios of probabilistic long-term vortex prediction under different levels of crosswinds, the wake separation and separation reduction compared to the RECAT-EU standard are demonstrated in Table 7. The separation is evaluated under minimum radar separation of 3 nautical miles and an average approach speed of 140 knots. It indicates that a strong crosswind of 5.9 m/s is able to reduce wake separation generated by aircraft in CAT-B to under 60 s, consequently reducing the approach separation for following aircraft in CAT-C and CAT-D to the minimum radar separation (MRS) by 25.9 s when compared to the separation in RECAT-EU standard. The second row shows that the separation reduction is more significant for lighter aircraft.

In addition, the vortex durations on the approach profiles were analysed statistically on the test dataset and wake sequences from January to April 2019, involving a total of 12,091 sequences and 2744 vortex sequences with mapped aircraft weight categories that are independent of the training dataset. Fig. 14 illustrates the transport of wake sequences in the test dataset under different levels of crosswinds, in which the colour represents the crosswind speed with directions, and the direction of the arrow indicates an increase in the timestep in the wake sequence. It is evident that the strong crosswinds are capable of removing entire wake pairs from the approach profiles at both runway entrances. Although the wake vortices may rebound with the increase in height, the lateral vortex movement is able to make the approach profile clear. The enlarged area shows that a large proportion of wake pairs with large lateral movement speeds are generated by aircraft in CAT-B and CAT-D categories, which provides evidence of separation reduction for heavy aircraft.

Table 8 lists the proportion of flights with potential separation reduction relative to the entire wake lifetime for each aircraft category. The number of flights whose wake separation could be shortened accounts for 27.33 % of the total. In addition, 91.06 % of flight separation reduction is generated when the absolute crosswind speed is over 2.5 m/s, indicating the effects of crosswind in lateral vortex transport. It is noteworthy to remark that when taking wake encounter risk analysis into consideration for determining the separation reduction, the proportion of flights with wake separation reduction may be further increased, especially for those under mean absolute crosswind of 0–3 m/s.

More specifically, Fig. 15 illustrates the predicted wake separation for flights in each aircraft category. The trend towards a shorter separation interval (the greatest separation) is evident as aircraft weight decreases. The separation time under absolute crosswind of 0–3 m/s, which also represents the worst-case wake encounter, is also compatible with the current RECAT-EU standard (see Appendix B). Nonetheless, when the absolute mean crosswind is over 5 m/s, the mean duration time of wake vortices on the approach profiles for all aircraft may be reduced to under 60 s. It is worth to mention that for wake pairs that always last in the approach profiles, the wake separation is taken as no reduction and as the same as their lifetime detected by the LiDAR, lacking consideration of wake encounter and its effect on separation reduction. Furthermore, the wake sequences over 12 timesteps are neglected. These may lead to an underestimation of the boundary values of the blue boxes for crosswinds between 0–3 m/s. More importantly, the actual flight separation will be the maximum between the predicted wake separation and the minimum radar separation, although the wake separation may be reduced to below 60 s.

Fig. 16 reveals wake separation reduction from the perspective of the proportion of aircraft numbers in each separation interval period. The time intervals in the x-axis represent the real duration of wake pairs with both vortices measured by LiDAR for the “Measurement” legend, while for the “Prediction” legend, they mean the predicted wake separation time by the DCNN-ATCN model. Fig. 16 (a) reveals that separation can be reduced for 21 % of wake vortices with a lifetime of at least 60–100 s to less than 60 s, and even below 40 s. Moreover, Fig. 16(b) shows that under a stable atmosphere (mean absolute crosswind of 0–3 m/s), the proportions of detected wake lifetime and predicted separation time in all time intervals are almost overlapped. These proportions peak between 80–100 s, indicating no evident separation reduction. Conversely, for a large proportion of wake pairs generated under absolute crosswind of 3–6 m/s with a lifetime of 60–80 s, their predicted wake separation time can be reduced to below 60 s, with the most significant proportion in the time interval of 40–60 s. Although the measured lifetime or predicted separation time may be under 60 s, the actual flight separation should be the maximum between predicted wake separation and the minimum radar separation.

6. Discussion

The present study demonstrated the performance of hybrid deep learning approaches in aircraft wake vortex feature mining, and the influence of crosswind in dynamic separation time in the final approach. In addition to the superior performance enhancement analysed previously, the managerial implementations of the proposed models and future work will be discussed in this section.

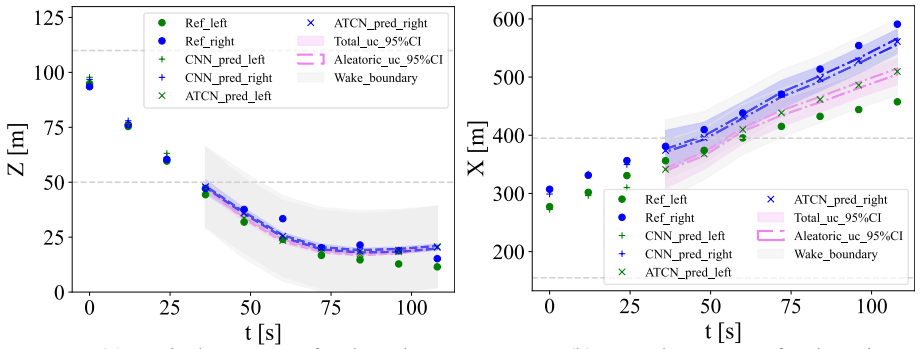

(a) Vertical transport of wake pair (b) Lateral transport of wake pair

Fig. 11. Visualisation of the long-term prediction results of the CNN-ATCN model of a vortex sequence generated by aircraft in the CAT-B category under mean crosswind of 2.08 m/s during 2019/07/14 15:08:55 – 15:10:45.

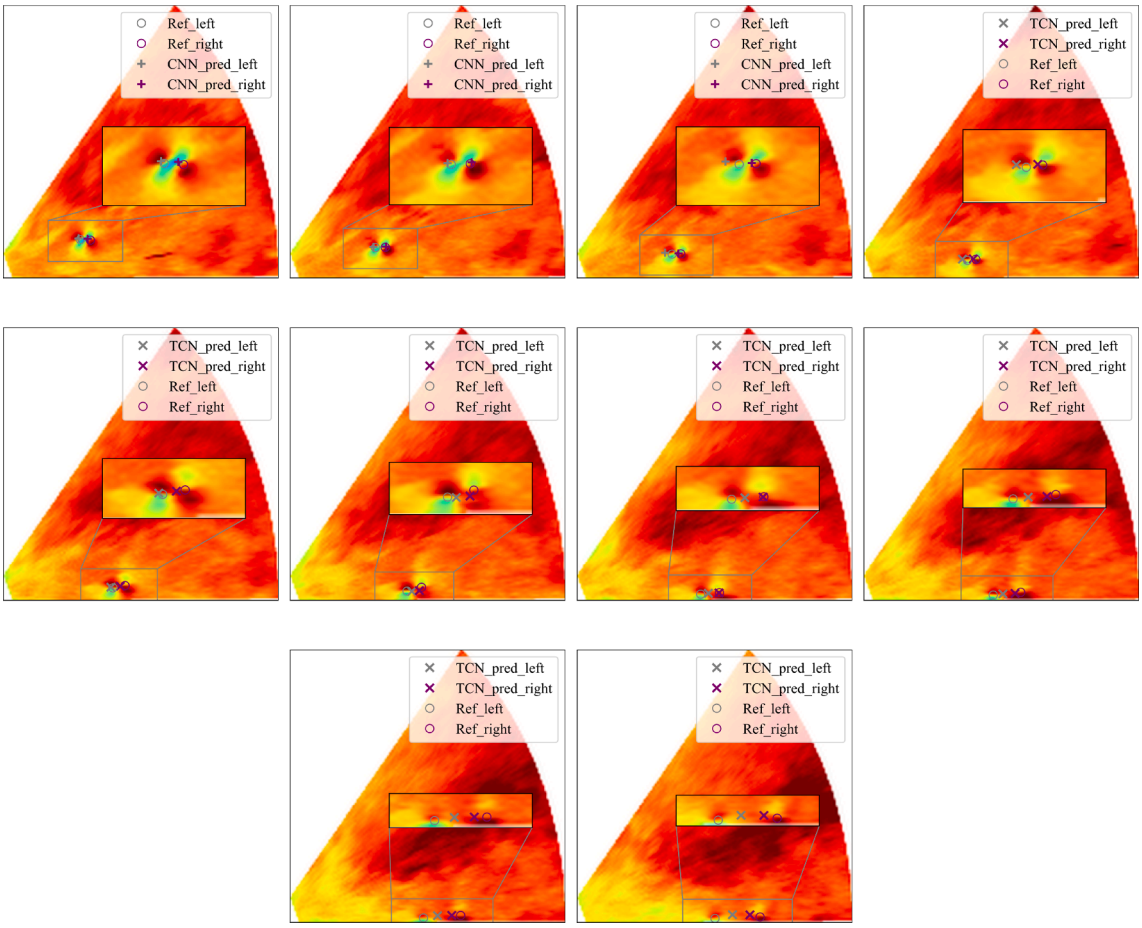

Fig. 12. Visualisation of the predicted results of Fig. 11 in LiDAR wake images.

6.1. Managerial implementations

This paper presents the fast-time data-driven methodology for dynamic flight separation suggestion in the final approach through near real-time aircraft wake vortex recognition and evolution prediction, using a hybrid deep learning framework. This research will foster more efficient and intelligent runway scheduling without sacrificing flight safety. The managerial implications of this research are described from three aspects:

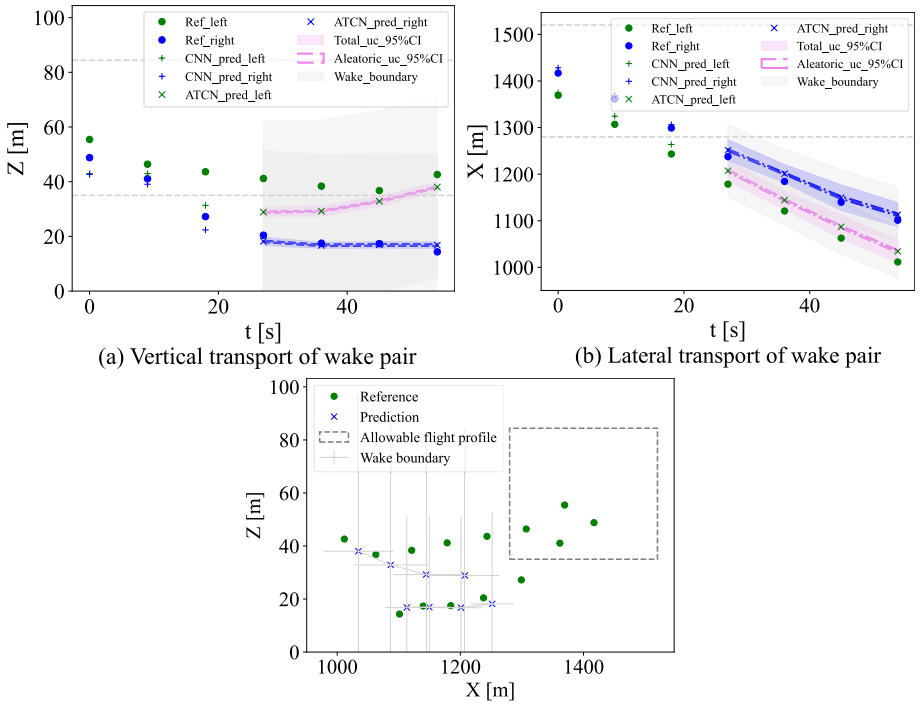

(a) Vertical transport of wake pair

(b) Lateral transport of wake pair

(c) Transport of wake pair in LiDAR scan plane

Fig. 13. Visualisation of the long-term prediction results of the CNN-ATCN model of a vortex sequence generated by aircraft in the CAT-D category in a mean crosswind of – 5.9 m/s during 2019/09/20 23:45:25 – 23:46:21.

Table 7
Scenarios of wake transport with dynamic separation reduction compared to the RECAT-EU standard.

Wake scenarios	Leading aircraft (Aircraft category)	Average approach speed	Average crosswind	Follower aircraft	Minimum DBS in RECAT	Minimum TBS in RECAT	Predicted wake duration	Minimum radar separation	Separation reduction
Fig. 9	A359 (B)	140 knots	0.23 m/s	CAT-D	4 NM	102.9 s	Over 120 s	3 NM/ 77 s	0
Fig. 11	A320 (D)	140 knots	2.08 m/s	CAT-F	5 NM	128.6 s	70 s /2.33 NM	3 NM/ 77 s	51.6 s
Fig. 13	A330 (B)	140 knots	−5.9 m/s	CAT-D	4 NM	102.9 s	35 s /1.17 NM	3 NM/ 77 s	25.9 s

Note: DBS refers to the distance-based separation, TBS represents the time-based separation, and NM refers to the nautical mile.

(1) **Support the development of wake vortex analysis models.** This paper presents a hybrid deep learning framework for on-board aircraft wake vortex recognition and evolution prediction, with considerable prediction accuracy and computation speed achieved. This will support the online monitoring of the vortex state and lifetime. Furthermore, this data-driven methodology can be ensembled with physical-based vortex modelling and simulation methods to enhance vortex prediction performance.

(2) **Support the construction of a dynamic flight separation system.** The potential of flight separation reduction is assessed based on the probabilistic results of vortex location prediction under vortex duration estimation. This exploratory flight separation evaluation with reliability analysis using data in real operational scenarios provides a promising idea for safety regulators in developing the time-based dynamic fight separation minima.

(3) **Improve runway operational efficiency and on-time performance.** The proposed wake prediction models may not directly support the advanced runway sequencing due to their limited prediction time horizon, but they may be applied to runway re-scheduling in near real-time situations. Next, the statistical analysis of flight separation reduction based on flight safety will benefit runway throughput and operational efficiency increase, especially during peak periods under optimisation of the traffic mix. For a specific arrival or departure sequence, the reduced flight separation also permits a reduction in the total flight time. This may provide air traffic controllers with additional flexibility in managing traffic. Furthermore, it will also allow for a more expeditious recovery from adverse weather or emergent situations, thereby reducing overall delays.

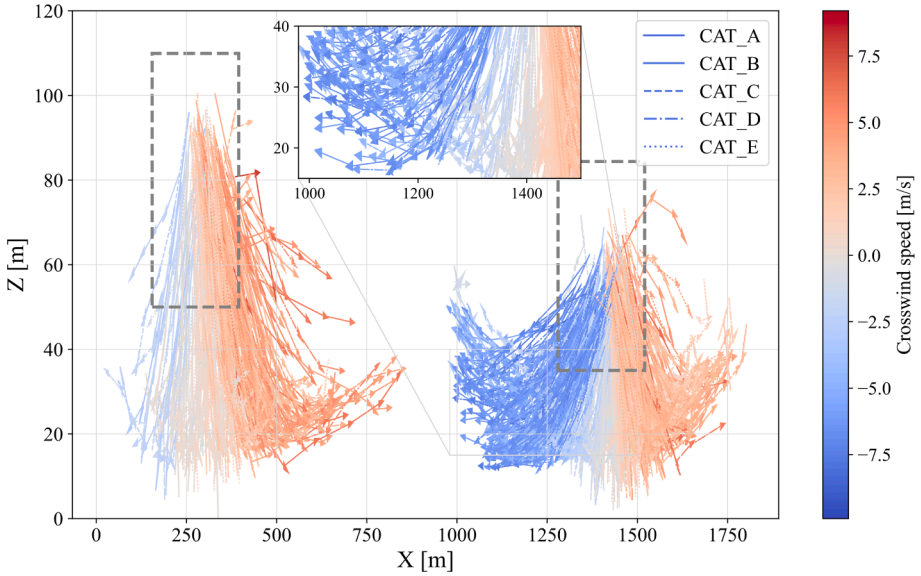

Fig. 14. Predicted transport of wake pairs in the test dataset under different mean crosswinds at Runway 25R and 07L.

Table 8
Proportion of flights with separation reduction under each aircraft weight category based on the long-term vortex location prediction.

Aircraft weight category	Proportion of flights with separation reduction	Proportion of flights under absolute crosswind speed over 2.5 m/s of the separation-reduced flights
CAT_A	34.48 %	**100 %**
CAT_B	23.6 %	99.22 %
CAT_C	22.95 %	92.85 %
CAT_D	**33.13 %**	81.46 %
CAT_E	**40 %**	**83.33 %**
Total flights	27.33 %	91.06 %

6.2. *Future work*

The evaluation of dynamic wake separation in this paper is an exploratory attempt, despite with the above reliability-improvement strategies to guarantee credibility. The potential and range of separation reduction are evaluated under the instrument landing procedure and approach profiles only in the LiDAR scan planes at the runway entrances. Furthermore, the background atmosphere conditions, which are a crucial factor in vortex transport, are considered in only the lateral direction and in a steady status in the entire vortex decay process. Due to the limitation of LiDAR's number, the crosswinds along the flight direction are also assumed to be the same and prevailing. Therefore, for situations of noticeable wind shear, headwind and dynamic crosswind along the flight direction, and other flight procedures, the duration time of aircraft wake vortices in the entire approach profiles, including the high airspace, deserves to be further optimised with additional data support. Furthermore, with more accurate wake strength estimation available, the separation reduction can also be verified from the perspective of wake encounter risk analysis for the wake pair always staying in the approach corridor.

Next, the ATCN and CNN-ATCN models proposed in this paper can only be implemented to predict future wake evolution at the minute level when the initial three-timestep wake features are known. These models may support the near real-time runway rescheduling. Nonetheless, to achieve more advanced runway sequencing hours in advance and under dynamic wake separation, the transport and duration of wake vortices in the approach path should be forecasted in a longer time horizon considering four-dimensional flight trajectory and dynamic wind prediction.

Finally, this paper proposes a data-driven deep-learning approach for forecasting the decay and transport of aircraft wake vortices. Although it indicates a considerable good fit with the LiDAR processing algorithm, other physical models and the CFD simulation can be used to verify or support the development of the deep learning approach and provide a more comprehensive analysis. It is also worth investigating methods to improve the model's generalization for handling complex situations where the LiDAR processing algorithm may fail.

7. Conclusion

Overall, a new data-driven fusion framework of deep learning is proposed for aircraft wake vortex recognition and decay

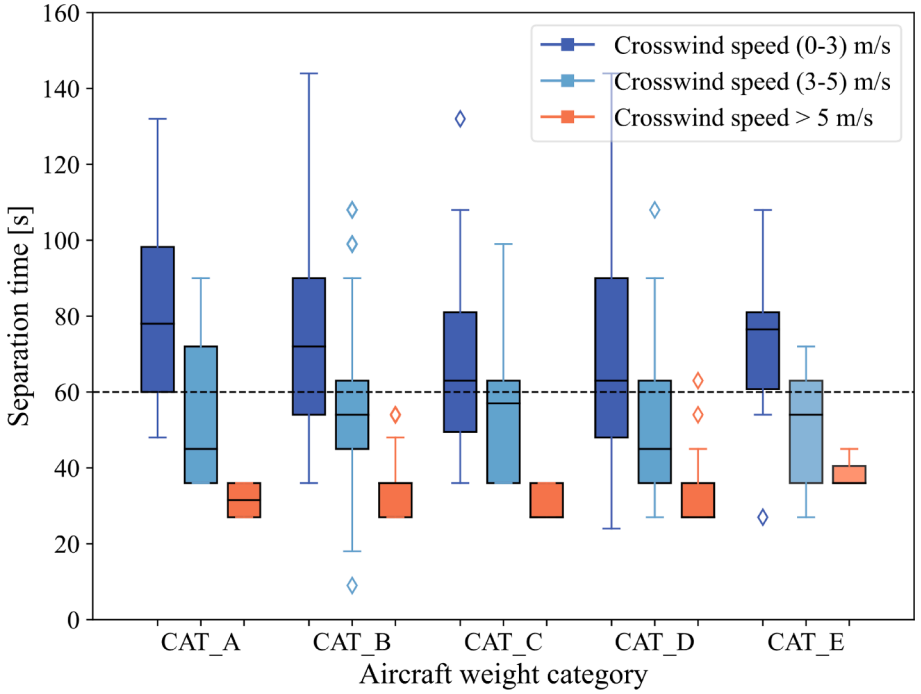

Fig. 15. Predicted wake separation minima under each aircraft weight category and different levels of mean absolute crosswinds.

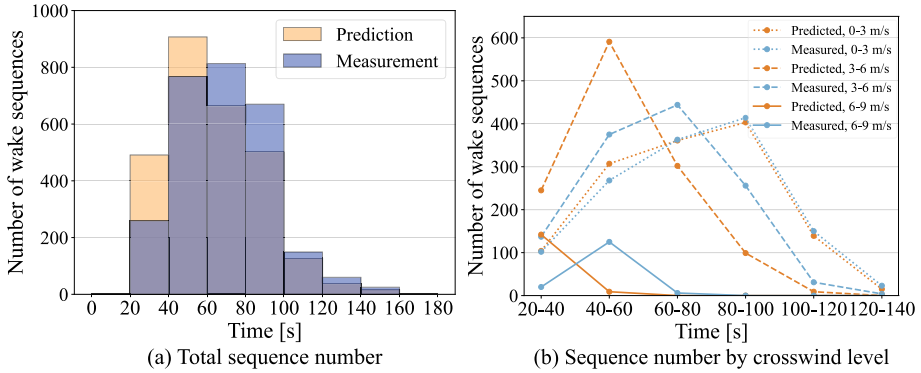

Fig. 16. Total number of wake sequences and wake sequences under different levels of mean absolute crosswinds by time interval of LiDAR measured lifetime or predicted separation time.

prediction, which provides a promising solution for wake vortex monitoring and duration assessment. In the offline stage, the two-stage deep convolutional networks that permit prompt and accurate identification of vortex locations and strength from wake vortex images are utilised for initial vortex recognition. Furthermore, we propose the probabilistic attention-based TCN models for vortex transport and decay forecasts, using historical spatiotemporal vortex data. Next, the DCNN and the ATCN model are integrated in sequence to realise online vortex recognition and future evolution prediction, combining the benefits of spatial feature analysis and temporal dependency identification. Finally, based on the predicted vortex locations with a high confidence level and duration assessment of vortex presence in the final approach profiles, the potential of dynamic flight separation minima is tentatively inferred for flights with aircraft in each weight category and under crosswind conditions.

As revealed in the performance indicators MAE and RMSE, the fusion of DCNN together with ATCN for forecasting aircraft wake vortices appears to be a promising solution. In addition, it provides a comprehensive view of spatial and temporal characteristics of current and future vortex locations. Moreover, the proposed the ATCN model outperforms specific state-of-the-art models substantially, especially for predicting the long-term movement of wake vortices. This framework achieves both outstanding prediction performance and low computational time. More importantly, the hybrid probabilistic models verify the potential of dynamic flight separation under crosswinds from several aspects.

Therefore, the benefit of fusing deep convolutional networks and attention-based temporal convolutional networks manifests in

three forms. It facilitates online and real-time aircraft wake vortex monitoring and duration evaluation. Next, it also supports the development of the dynamic flight separation system. Finally, the dynamic separation time indicated over this framework also facilitates runway rescheduling and near rea-time scheduling for improving runway operational capacity and efficiency.

CRediT authorship contribution statement

Nana Chu: Data curation, Formal analysis, Investigation, Methodology, Writing – original draft. **Kam K.H. Ng:** Conceptualization, Funding acquisition, Investigation, Methodology, Project administration, Resources, Supervision, Writing – review & editing. **Xinting Zhu:** Formal analysis, Investigation, Methodology, Validation, Visualization, Writing – review & editing. **Ye Liu:** Data curation, Resources, Software, Visualization, Writing – review & editing. **Lishuai Li:** Data curation, Formal analysis, Investigation, Supervision, Validation, Writing – review & editing. **K.K. Hon:** Conceptualization, Data curation, Formal analysis, Investigation, Project administration, Resources, Software.

Declaration of Competing Interest

The authors declare that they have no known competing financial interests or personal relationships that could have appeared to influence the work reported in this paper.

Data availability

The authors do not have permission to share data.

Acknowledgement

The work described in this paper was supported by grants from the Research Grants Council, the Hong Kong Government (Grant No. PolyU25218321, PolyU15201423), Department of Aeronautical and Aviation Engineering, The Hong Kong Polytechnic University, Hong Kong SAR (RJ8N, RJ78), and the National Natural Science Foundation of China (Grant number: 72301229).

Appendix A. . Optimal model configuration

1. Attention-based TCN models

The four residual temporal convolutional modules in the proposed TCN models are comprised of one-dimensional causal dilated convolutional layers with dilation rates of 0, 2, 4 and 8, respectively, and 64 filters with a kernel size of 2 in each layer. The dropout rate in these modules is 0.2.

The multi-head attention mechanism in this model is defined under 16 heads and a total 64 neurons of the dense layer for linear projection of Q, K, V vectors. The channel attention in the CBAM module is constructed under one dense layer with 32 neurons and activation function of Rectified Linear Units, and another dense layer with 64 neurons for vector reshaping.

In the decoder part of the model, the global max-pooling layer extracts the most salient features across the temporal dimension and reduces the output to a fixed-size representation, followed by one dense layer with 128 neurons and another dense layer that produces the output.

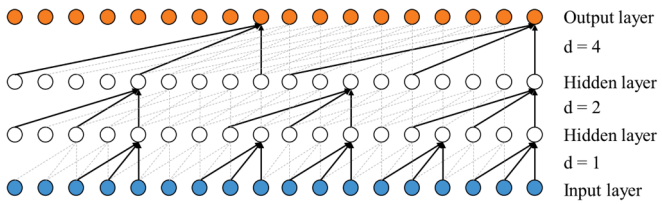

Fig. 17. Graphical representation of dilated convolutions with dilation factors and filter size of 3.

2. Uncertainty modelling

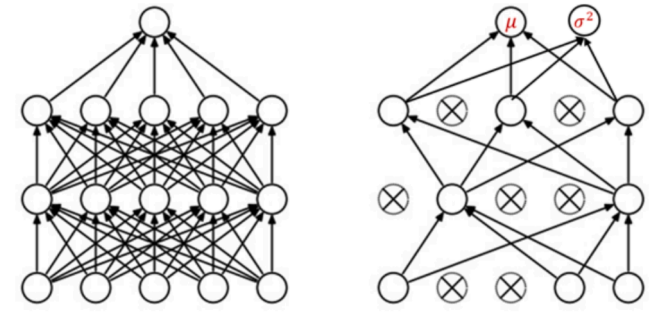

Fig. 18. Modelling of aleatoric uncertainty and epistemic uncertainty.

As illustrated in Fig. 18, compared to the network with all neurons trained and deterministic single output, the aleatoric uncertainty is learned in this work by allowing the model to output probability distributions instead of deterministic point predictions, which inherently incorporates the aleatoric uncertainty in the data.

$$\mathrm{p}(\mathrm{y}|\mathrm{x},\Theta) = N(y|f(x,\Theta),\ \sigma^2) \tag{11}$$

Where the network weights are denoted as Θ. The training data D is $\{(\mathrm{x}_1,\mathrm{y}_1),(\mathrm{x}_2,\mathrm{y}_2),\cdots,(\mathrm{x}_\mathrm{n},\mathrm{y}_\mathrm{n})\}$, where x_i represents input sample, y_i is corresponding target output, and $f(x_i,\Theta)$ represents the network. The $N(y|f(x,\Theta),\ \sigma^2)$ represents the Gaussian distribution with mean model output $f(x,\Theta)$ and variance σ^2.

The epistemic uncertainty focuses on estimating the posterior distribution of Θ, given the observed dataset D:

$$\mathrm{p}(\Theta|\mathrm{D}) = \frac{\mathrm{p}(\mathrm{D}|\Theta)*\mathrm{p}(\Theta)}{p(D)} \tag{12}$$

Where $\mathrm{p}(\mathrm{D}|\Theta)$ is the likelihood function, $\mathrm{p}(\Theta)$ is the prior distribution of Θ, and $p(D)$ is the marginal likelihood.

Importantly, it has been demonstrated that the Monte Carlo Dropout has a similar effect in minimising KL divergence, so as to approximate the posterior distribution (Gal and Ghahramani, 2016). Consequently, with the estimated posterior distribution, probabilistic outputs can be made by averaging the predictions from multiple dropout samples. The probabilistic distribution of the model on new data x^* can therefore be generated by integrating over θ and estimated with MC samples, in which K is the number of MC samples:

$$p(y^*|x^*,X,Y) = \int p(y^*|x^*,\Theta)p(\Theta|X,Y)d\Theta \approx \frac{1}{K}\sum_{n=1}^{K} p\left(y^*\middle|x^*,\widetilde{\Theta}_k\right) \tag{13}$$

3. Benchmarking models

For wake decay prediction, the LSTM model and GRU model are taken as benchmarks. These two models contain two layers with 64 and 32 neurons with a dropout rate of 0.2.

Appendix B. -Flight standards and dynamic separation results

.

Table 9
ICAO wake separation minima under categories of maximum take-off mass.

Leader/ Follower (NM)	A380	Heavy	Medium	Light
A380	MRS	6	7	8
Heavy	MRS	4	5	6
Medium	MRS	MRS	MRS	5
Light	MRS	MRS	MRS	MRS

Note: MRS refers to the minimum radar separation, which remains 2.5/3NM, and NM represents the nautical mile.

Table 10
RECAT-EU distance-based separation minima on approach.

Leader/ Follower (NM)		Super heavy	Upper heavy	Lower heavy	Upper medium	Lower medium	Light
		A	B	C	D	E	F
Super heavy	A	3	4	5	5	6	8
Upper heavy	B	MRS	3	4	4	5	7
Lower heavy	C	MRS	MRS	3	3	4	6
Upper medium	D	MRS	MRS	MRS	MRS	MRS	5
Lower medium	E	MRS	MRS	MRS	MRS	MRS	4
Light	F	MRS	MRS	MRS	MRS	MRS	3

References

Balakrishnan, H., Chandran, B.G., 2010. Algorithms for scheduling runway operations under constrained position shifting. Oper. Res. 58 (6), 1650–1665.

Barea, A., de Celis, R., Cadarso, L., 2024. An integrated model for airport runway assignment and aircraft trajectory optimisation. Transp. Res. Part C: Emerg. Technol. 160, 104498.

Breitsamter, C., 2011. Wake vortex characteristics of transport aircraft. Prog. Aerosp. Sci. 47 (2), 89–134.

Burnham, D.C., Hallock, J.N., 1982. Chicago monostatic acoustic vortex sensing system: Vol. IV. wake vortex decay. (No. DOT/FAA/RD-79-103, IV). United States. Department of Transportation. Federal Aviation Administration.

Chu, N., Ng, K.K.H., Liu, Y., Hon, K.K., Chan, P.W., Li, J., Zhang, X., 2024. Assessment of approach separation with probabilistic aircraft wake vortex recognition via deep learning. Transp. Res. Part E: Log. Transport. Rev. 181, 103387.

Chung, J., Gulcehre, C., Cho, K., Bengio, Y., 2014. Empirical evaluation of gated recurrent neural networks on sequence modeling. arXiv preprint arXiv:1412.3555.

De Visscher, I., Winckelmans, G., Treve, V., 2015. A simple wake vortex encounter severity metric: Rolling moment coefficient due to encounter of an aircraft with a wake vortex.

De Visscher, I., Treve, V., Winckelmans, G., 2016. Characterization of Aircraft Wake Vortex Circulation Decay in Reasonable Worst Case Conditions, *54th AIAA Aerospace Sciences Meeting*. Am. Inst. Aeronautics and Astronautics.

Diana, T., 2015. An evaluation of departure throughputs before and after the implementation of wake vortex recategorization at Atlanta Hartsfield/Jackson International Airport: a Markov regime-switching approach. Transp. Res. Part E: Log. Transport. Rev. 83, 216–224.

DSAN, 2018. A fine-tuned wake vortex recategorisation at Paris-CDG & Le Bourget Airports to optimise sequencing on arrival. Maurice Georges.

EUROCONTROL, 2018. European wake turbulence categorisation and separation minima on approach and departure. EUROCONTROL Headquarters, Brussels.

EUROCONTROL, 2023. Approach and departure optimised wake turbulence re-categorisation and pair-wise separation minima, 2.0 ed.

FAA, 2016. Wake Turbulence Recategorization. Federal Aviation Administration, Washington, DC.

FAA, 2020. NextGen Annual Report. U.S. Department of Transportation.

Gal, Y., Ghahramani, Z., 2016. Dropout as a bayesian approximation: representing model uncertainty in deep learning. Int. Conf. Mach. Learn. PMLR 1050–1059.

Hallock, J.N., Holzäpfel, F., 2018. A review of recent wake vortex research for increasing airport capacity. Prog. Aerosp. Sci. 98, 27–36.

Hochreiter, S., Schmidhuber, J., 1997. Long short-term memory. Neural Comput. 9 (8), 1735–1780.

Holzäpfel, F., 2003. Probabilistic two-phase wake vortex decay and transport model. J. Aircr. 40 (2), 323–331.

Holzäpfel, F., 2006. Probabilistic two-phase aircraft wake-vortex model: further development and assessment. J. Aircr. 43 (3), 700–708.

Holzäpfel, F., Gerz, T., Köpp, F., Stumpf, E., Harris, M., Young, R.I., Dolfi-Bouteyre, A., 2003. Strategies for circulation evaluation of aircraft wake vortices measured by lidar. J. Atmos. Oceanic Tech. 20 (8), 1183–1195.

Holzäpfel, F., Steen, M., 2007. Aircraft wake-vortex evolution in ground proximity: analysis and parameterization. AIAA J. 45 (1), 218–227.

Holzäpfel, F., Strauss, L., Schwarz, C., 2021. Assessment of dynamic pairwise wake vortex separations for approach and landing at Vienna airport. Aerosp. Sci. Technol. 112, 106618.

Hon, K.K., Chan, P.W., Chim, K.C.Y., De Visscher, I., Thobois, L., Rooseleer, F., Troiville, A., 2021. Wake vortex measurements at the Hong Kong International Airport, *AIAA SCITECH 2022 Forum*. Am. Inst. Aeronautics and Astronautics.

IATA, 2022. Climate change. International Civil Aviation Organisation.

ICAO, 2023. Enhanced wake turbulence separation webinar for the APAC Region.

Köpp, F., Rahm, S., Smalikho, I., Dolfi, A., Cariou, J.P., Harris, M., Young, R.I., 2005. Comparison of wake-vortex parameters measured by pulsed and continuous-wave lidars. J. Aircr. 42, 916–923.

Lea, C., Vidal, R., Reiter, A., Hager, G.D., 2016. Temporal convolutional networks: A unified approach to action segmentation, *Computer Vision–ECCV 2016 Workshops: Amsterdam, The Netherlands, October 8-10 and 15-16, 2016, Proceedings, Part III 14*. Springer, pp. 47-54.

Li, J., Shen, C., Gao, H., Chan, P.W., Hon, K.K., Wang, X., 2020. Path integration (PI) method for the parameter-retrieval of aircraft wake vortex by Lidar. Opt. Express 28 (3), 4286–4306.

Lin, M., Huang, W., Zhang, Z., Xu, C., Cui, G., 2017. Numerical study of aircraft wake vortex evolution near ground in stable atmospheric boundary layer. Chin. J. Aeronaut. 30 (6), 1866–1876.

Lundberg, S.M., Lee, S.-I., 2017. A unified approach to interpreting model predictions. Adv. Neural Information Process. Syst. 30.

NATS, 2018. Enhanced time-based separation for Heathrow arrivals & RECAT-EU for arrivals and departures.

Ng, K.K.H., Lee, C.K.M., Chan, F.T.S., Chen, C.-H., Qin, Y., 2020. A two-stage robust optimisation for terminal traffic flow problem. Appl. Soft Comput. 89, 106048.

Pan, W., Wu, Z., Zhang, X., 2020. Identification of aircraft wake vortex based on SVM. Math. Probl. Eng. 2020, 9314164.

Pang, Y., Zhao, X., Yan, H., Liu, Y., 2021. Data-driven trajectory prediction with weather uncertainties: a Bayesian deep learning approach. Transp. Res. Part C: Emerg. Technol. 130, 103326.

Pang, Y., Zhao, P., Hu, J., Liu, Y., 2024. Machine learning-enhanced aircraft landing scheduling under uncertainties. Transp. Res. Part C: Emerg. Technol. 158, 104444.

Prakash, R., Piplani, R., Desai, J., 2018. An optimal data-splitting algorithm for aircraft scheduling on a single runway to maximize throughput. Transp. Res. Part C: Emerg. Technol. 95, 570–581.

Proctor, F., 1998. The NASA-Langley wake vortex modelling effort in support of an operational aircraft spacing system In: 36th AIAA Aerospace Sciences Meeting and Exhibit.

Robins, R.E., Delisi, D.P., 1996. 3-D Calculations Showing the Effects of Stratification on the Evolution of Trailing Vortices. In: Deville, M., Gavrilakis, S., Ryhming, I.L. (Eds.), Computation of Three-Dimensional Complex Flows. Vieweg+Teubner Verlag, Wiesbaden, pp. 264–270.

Samà, M., D'Ariano, A., Corman, F., Pacciarelli, D., 2017. Metaheuristics for efficient aircraft scheduling and re-routing at busy terminal control areas. Transp. Res. Part C: Emerg. Technol. 80, 485–511.

SESAR, 2015. Capacity gains with time-based arrivals.

Shafienya, H., Regan, A.C., 2022. 4D flight trajectory prediction using a hybrid Deep Learning prediction method based on ADS-B technology: a case study of Hartsfield-Jackson Atlanta International Airport (ATL). Transp. Res. Part C: Emerg. Technol. 144, 103878.
Shen, C., Tang, W., Gao, H., Wang, X., Chan, P.W., Hon, K.K., Li, J., 2023. Aircraft wake recognition and strength classification based on deep learning. IEEE J. Sel. Top. Appl. Earth Obs. Remote Sens. 16, 2237–2249.
Shi, Z., Xu, M., Pan, Q., 2021. 4-D flight trajectory prediction with constrained LSTM network. IEEE T Intell. Transp. 22 (11), 7242–7255.
Smalikho, I.N., 2019. Taking into account the ground effect on aircraft wake vortices when estimating their circulation from lidar measurements. Atmos. Oceanic Opt. 32 (6), 686–700.
Smalikho, I.N., Banakh, V.A., 2015. Estimation of aircraft wake vortex parameters from data measured with a 1.5-μm coherent Doppler lidar. Opt. Lett. 40 (14), 3408–3411.
Smalikho, I.N., Banakh, V.A., Holzäpfel, F., Rahm, S., 2015. Method of radial velocities for the estimation of aircraft wake vortex parameters from data measured by coherent Doppler lidar. Opt. Express 23 (19), A1194–A1207.
Thobois, L.P., Krishnamurthy, R., Cariou, J.-P., Nicolaon, J.P., 2016. Deployment of a next generation and operational LIDAR solution for monitoring wake vortices for supporting new wake turbulence regulations (Invited), *8th AIAA Atmospheric and Space Environments Conference*. Am. Inst. Aeronautics and Astronautics.
Visscher, I.D., Bricteux, L., Winckelmans, G., 2013. Aircraft vortices in stably stratified and weakly turbulent atmospheres: simulation and modeling. AIAA J. 51 (3), 551–566.
Visscher, I.D., Winckelmans, G., Lonfils, T., Bricteux, L., Duponcheel, M., Bourgeois, N., 2010. The WAKE4D Simulation Platform for Predicting Aircraft Wake Vortex Transport and Decay: Description and Examples of Application In: AIAA Atmospheric and Space Environments Conference.
Wartha, N., Stephan, A., Holzäpfel, F., Rotshteyn, G., 2022. Characterizing aircraft wake vortex position and strength using LiDAR measurements processed with artificial neural networks. Opt. Express 30 (8), 13197–13225.
Woo, S., Park, J., Lee, J.-Y., Kweon, I.S., 2018. CBAM: Convolutional Block Attention Module. In: Ferrari, V., Hebert, M., Sminchisescu, C., Weiss, Y. (Eds.), Computer Vision – ECCV 2018. Springer International Publishing, Cham, pp. 3–19.
Wu, S., Zhai, X., Liu, B., 2019. Aircraft wake vortex and turbulence measurement under near-ground effect using coherent Doppler lidar. Opt. Express 27 (2), 1142–1163.
Xu, Z., Li, D., Cai, J., 2023. Long-wave deformation of in-ground-effect wake vortex under crosswind condition. Aerosp. Sci. Technol. 142, 108697.
Yoshikawa, E., Matayoshi, N., 2017. Aircraft wake vortex retrieval method on lidar lateral range-height indicator observation. AIAA J. 55 (7), 2269–2278.